

Resonance of long waves generated by storms obliquely crossing shelf topography in a rotating ocean

S. THIEBAUT[†] AND R. VENNELL

Ocean Physics Group, Department of Marine Science, University of Otago, Dunedin 9054,
New Zealand

(Received 17 December 2010)

The oceanic forced wave beneath a moving atmospheric disturbance is amplified by Proudman resonance. When modified by the Earth's rotation this classical resonance only occurs if the disturbance time scale is smaller than the inertial period. With or without Coriolis effects free transients generated by storm forced waves obliquely crossing step changes in water depth at particular angles are shown to resonate by exciting a range of barotropic free waves. Rotationally influenced slow atmospherically forced waves crossing a vertical coast at a critical angle lead to a form of sub-critical resonance, which occurs only when the component of the disturbances' phase velocities along the coast matches that of a free Kelvin wave (KW). In a rotating ocean transients generated by disturbances crossing a step at a particular angle are shown to excite a free double Kelvin wave (DKW). This new type of resonance only occurs for sufficiently large steps and disturbances with time scale greater than the inertial period. A storm crossing a step shelf can result in the excitation of an infinite set of edge-waves, a single KW, a unique DKW and a first-mode continental shelf wave, depending on the topography and the disturbance time scale, translation speed and incident angle. The study of resonances and wave mode excitations generated by storms crossing a coast or a continental shelf may contribute to understanding how a particular combination of the storm characteristics can result in destructive coastal events with time scales encompassing the typical meteotsunami period band (tens of minutes) and storm surges with periods of several hours or days.

1. Introduction

The forced wave generated by a moving atmospheric disturbance can be amplified by the well-known Proudman resonance when the translation speed of the disturbance approaches the shallow water wave speed (i.e. at critical translation speed) (Lamb 1932; Proudman 1953). A disturbance travelling parallel to the coast over a linearly sloping bottom can also lead to a large forced ocean wave amplification due to Greenspan resonance (Greenspan 1956). This is due to the excitation of one of the coastally trapped edge-wave modes, and is large at critical disturbance speeds (Greenspan 1956). Garrett (1970) showed how free waves can be generated when a fast super-critical atmospheric disturbance crosses a step. He noted the possibility of typically slow moving weather systems crossing ridges and creating free waves, commenting that they would be too small to be detected, though Vennell (2007) (hereafter V07) showed that transient free waves of significant amplitudes can be generated by small fast-moving storms moving across shelves and ridges. Vennell (2010) (hereafter V10) showed that a sub-critical resonance

[†] Email address for correspondence: thise135@student.otago.ac.nz

occurs when a relatively slow moving forced wave in a flat-bottomed ocean crosses a vertical coast at a particular angle and may enhance coastal surges under sub-critical storms. Here it is shown that including rotational effects gives a more complex sea level response and results in broader applicability of the model. Rotationally influenced forced waves crossing step changes in water depth at critical angles can resonate by exciting four different types of trapped free waves.

Proudman and Greenspan resonances and that of V10 are based on the assumption that the effects of the Earth's rotation can be neglected. This is possible if the time scale of the disturbance (i.e. the passage time of the disturbance over a fixed point) is small compared to the inertial period. V07 and V10 contributed to understanding how atmospheric disturbances of short time scales may excite shelf seiches and large transient waves which can result in destructive meteotsunami events (within the 5–30 min period band) at several locations around the world (Nomitsu 1935; Defant 1961; Monserrat *et al.* 1991; Rabinovich & Monserrat 1996; Monserrat *et al.* 2006; Vilibić *et al.* 2008; Goring 2009). Here it is shown that conditions for the occurrence of Proudman resonance and that suggested by V10 are modified in the presence of Coriolis effects. Modified Proudman Resonance (MPR) was implicitly formulated by Gill (1982, p. 348). This study proposes a better understanding of how more common storm induced surges may arise from disturbances which have time scales much longer than the typical meteotsunami period band.

Thomson (1970) found that only the longshore component of the wind-stress and pressure gradient can generate Kelvin-type waves, in agreement with Kajiura (1962). Thomson (1970) considered a semi-infinite ocean of constant depth bounded by a vertical wall and studied the responses to a non-travelling wind stress pattern (with only an alongshore component) and to a storm travelling in the alongshore direction, allowing the generation of Kelvin waves (KW) only for critical disturbance speeds. Here the general case of travelling wind stress and atmospheric pressure forcing is explored and shows that the KW mode can be excited by sub-critical storms impacting the coast with a particular angle.

Longuet-Higgins (1968a) discovered the existence of double Kelvin waves (DKWs) trapped along a discontinuity in depth. Here a forced wave, with period greater than the inertial period and crossing a step with a particular angle in a rotating ocean, is shown to lead to a sub-inertial resonance responsible for the excitation of a DKW. Mysak (1969) showed analytically how a transient or time-periodic nondivergent wind stress field, with a component only in the direction normal to the discontinuity in depth, can generate DKWs. This paper demonstrates that a travelling wind stress and/or atmospheric pressure disturbance leads to a new type of sub-inertial resonance for a particular forcing incident angle and a sufficiently large step.

Robinson (1964) and Mysak (1967a,b) suggested that the generation of continental shelf waves might be due to a resonant response of the sea surface to atmospheric pressure disturbances. However, opinion rapidly favoured the generation of shelf waves by the wind stress (Buchwald & Adams 1968; Adams & Buchwald 1969; Gill & Schumann 1974; LeBlond & Mysak 1978; Gill 1982). Several observational and/or numerical studies showed that the ocean response after the passage of a storm over a shelf can be either in the form of super-inertial edge waves (Lighthill 1998; Mercer *et al.* 2002; Yankovsky 2008, 2009; V10; and others) or sub-inertial shelf waves (Gordon & Huthnance 1987; Xie *et al.* 1999; Teague *et al.* 2007; Thiebaut & Vennell 2010; and others). It is shown here that a forced wave moving over an idealized step shelf is able to excite an infinite set of super-inertial edge wave modes and a unique sub-inertial shelf wave mode described by Munk *et al.* (1970).

The Saffir–Simpson hurricane scale was developed to provide a simple method for estimating storm surges and damage potential as a simple function of the maximum wind speed within a hurricane (e.g. Simpson 1974). Irish *et al.* (2008) used a numerical model to show that storm size also plays a key role in surge generation in coastal areas, with a greater enhancement for large hurricanes. Weisberg & Zheng (2006) studied numerically the influence of the hurricane intensity, landfall location, forward speed, and direction on simulated hurricane surges within a bay and concluded that the surge response was sensitive to all of these parameters. This paper shows analytically how a particular combination of the storm translation speed (relative to the depth), time scale and direction can generate a resonant response of the ocean and enhance the storm surge as the disturbance crosses a vertical coast, a step or a shelf.

The linearized forced and free shallow water equations in a rotating ocean are developed in section 2. Section 3,4 and 5 give solutions for the forced wave crossing a coast, a step and a shelf, respectively. Several events related to the model results are discussed in section 6.

2. The analytic model

2.1. Forced wave solutions

A two-dimensional barotropic ocean model for transient shallow water waves generated by a moving atmospheric disturbance over varying topography is developed. The disturbance time scale $T_p = L/U$ (where L is its width, and U its translation speed) is assumed to be comparable to the inertial period so that Coriolis effects must be taken into account. The depth is assumed to be large enough to neglect bottom friction. Hydrostatic balance gives the pressure at any depth $-z$ (z is measured vertically upwards) as $p = \rho g(\eta - z) + p_a$ where η is the displacement of the ocean's surface, ρ is the ocean water density, g is the acceleration of gravity, $p_a = -\rho g \eta_a$ is the atmospheric pressure at the ocean's surface due to the disturbance and η_a is the ocean's surface displacement under a stationary disturbance. The linearized atmospherically forced barotropic two-dimensional governing equations in a horizontal Cartesian co-ordinate system (x,y) for shallow water motion in constant water depth h are (e.g. Thomson 1970)

$$\frac{\partial u}{\partial t} - fv = -g \frac{\partial \eta}{\partial x} + g \frac{\partial \eta_a}{\partial x} + \frac{\tau^x}{\rho h}, \quad (2.1)$$

$$\frac{\partial v}{\partial t} + fu = -g \frac{\partial \eta}{\partial y} + g \frac{\partial \eta_a}{\partial y} + \frac{\tau^y}{\rho h}, \quad (2.2)$$

$$\frac{\partial \eta}{\partial t} + h \left(\frac{\partial u}{\partial x} + \frac{\partial v}{\partial y} \right) = 0, \quad (2.3)$$

where u and v are the velocity components of the fluid, (τ^x, τ^y) are the components of wind stress, f is the constant Coriolis parameter (chosen to correspond to latitude 45°N) and η is assumed small compared to the water depth. Combining (2.1)-(2.3) gives

$$\frac{\partial^2 \eta}{\partial t^2} - c^2 \nabla^2 \eta + fh\zeta = -c^2 \nabla^2 \eta_a + \frac{1}{\rho} \nabla \cdot \tau, \quad (2.4)$$

where $c = \sqrt{gh}$, $\nabla^2 = (\partial^2/\partial x^2) + (\partial^2/\partial y^2)$ and $\zeta = (\partial v/\partial x) - (\partial u/\partial y)$ is the relative vorticity of the fluid.

The time derivative of (2.4) combined with the y - and x -derivative of (2.1) and (2.2),

respectively, and (2.3) yield, after integrating with respect to time:

$$\frac{\partial^2 \eta}{\partial t^2} - c^2 \nabla^2 \eta + f^2 \eta = -c^2 \nabla^2 F, \quad (2.5)$$

where the forcing term is a combination of the atmospheric pressure and the wind stress forcing as

$$\frac{\partial}{\partial t} \nabla^2 F = \frac{\partial}{\partial t} \nabla^2 \eta_a - \frac{1}{\rho c^2} \frac{\partial}{\partial t} \nabla \cdot \tau + \frac{f^2}{c^2} w_E, \quad (2.6)$$

in which $w_E = (\rho f)^{-1} \nabla \times \tau$ is the Ekman pumping. The combined forcing due to a periodic disturbance of angular frequency ω , wavenumber $K_F = \sqrt{k_F^2 + l_F^2}$ (k_F and l_F are the x - and y -components of K_F , respectively), translation speed $U = \omega/K_F$ and wavelength $L = 2\pi/K_F$ (which conceptually defines the storm width) can be expressed as

$$F = F_0 \exp [i (k_F x + l_F y - \omega t)], \quad (2.7)$$

for which the steady-state forced wave solution to (2.5) has the form

$$\eta_F = \eta_{F0} \exp [i (k_F x + l_F y - \omega t)], \quad (2.8)$$

where $\eta_{F0} = F_0 / (1 - Fr^2 + \tilde{L}^2)$ in which $Fr = U/c = \omega / (cK_F)$ is the Froude number and $\tilde{L} = f / (cK_F) = L / (2\pi L_r)$ is the dimensionless disturbance width (which gives the width of the disturbance, L , relative to the Rossby Radius of deformation $L_r = c/f$).

The forcing terms in (2.6) can be written as:

$$\eta_a = \eta_{a0} \exp [i (k_F x + l_F y - \omega t)] \quad (2.9)$$

$$(\tau^x, \tau^y) = (\tau_0^x, \tau_0^y) \exp \{i [k_F x + l_F y - \omega t + \mu]\} \quad (2.10)$$

where μ is the phase difference between the ocean's surface response to atmospheric pressure and wind forcing, varying between 0 (for an extremely fast moving disturbance) and $\text{sgn}(f)\pi/2$ (assuming the air is in geostrophic balance). The choice of μ does not affect the general model results and the simple case of $\mu = \pi/2$ is chosen here. Thus F_0 can be expressed as the sum of atmospheric pressure and wind forcing

$$F_0 = \eta_{a0} + F_{0\tau}, \quad (2.11)$$

where

$$F_{0\tau} = \frac{1}{\rho c^2 K_F^2} \left[(k_F \tau_0^x + l_F \tau_0^y) - i \frac{f}{\omega} (k_F \tau_0^y - l_F \tau_0^x) \right]. \quad (2.12)$$

A comparison of the wind with atmospheric pressure effects on the sea level under the forced wave demonstrates that wind effects are generally largely dominant (not shown), in agreement with for instance Gill (1982, p. 340) who neglected the divergence of the wind stress. Equation (2.12) shows that the divergence of the wind stress ' $(k_F \tau_0^x + l_F \tau_0^y)$ ' has some importance for higher frequency disturbances. The terms related to the Ekman pumping ' $(k_F \tau_0^y - l_F \tau_0^x)$ ' become more important for low-frequency disturbances, i.e. $\omega/f < 1$.

Transient free waves are generated by the interaction of the barotropic velocity, associated with the forced wave, with the topography. With a view to determining the boundary conditions for different topographies oriented parallel to the y axis, (2.1) and (2.2) give the cross-topographic velocity associated with the forced wave as

$$u_F = \frac{g(\mathcal{F}_{\eta_a} + \mathcal{F}_\tau)}{(1 - Fr^2 + \tilde{L}^2)(\omega^2 - f^2)} \exp [i (k_F x + l_F y - \omega t)], \quad (2.13)$$

where

$$\mathcal{F}_{\eta_a} = \eta_{a0} \left(Fr^2 - \tilde{L}^2 \right) (\omega k_F + i f l_F) \text{ and} \quad (2.14)$$

$$\mathcal{F}_\tau = F_{0\tau} (\omega k_F + i f l_F) - (\rho g h)^{-1} (\omega \tau_0^x + i f \tau_0^y) \left(1 - Fr^2 + \tilde{L}^2 \right) \quad (2.15)$$

are forcing functions linked to atmospheric pressure and wind stress effects, respectively. For convenience, the sum of those functions is written $\mathcal{F} = \mathcal{F}_{\eta_a} + \mathcal{F}_\tau$ hereafter.

2.2. Storm characteristics used in presented examples

An arbitrary value of hydrostatic response of the ocean, η_a , of 0.6 m (assuming that it corresponds to approximately 60 hPa change in air pressure, e.g. Doodson 1924) is used in this study to simulate strong storm conditions (e.g. Gordon & Huthnance 1987; Tang *et al.* 1998). Assuming the atmospheric disturbance is in gradient wind balance and without forward motion, the wind speed $W(r)$ as a function of distance r from the storm center is given by (Holland 1980)

$$W(r) = \left\{ \frac{A}{r^B} \frac{B \Delta p}{\rho_a} \exp\left(-\frac{A}{r^B}\right) + \frac{r^2 f^2}{4} \right\}^{\frac{1}{2}} - \frac{r f}{2} \quad (2.16)$$

where A and B are scaling parameters, ρ_a is the air density (1.15 kg m^{-3}) and Δp is the difference between the hurricane central atmospheric pressure and the ambient atmospheric pressure. Assuming the air is in cyclostrophic balance (i.e. the Coriolis force is small compared to the pressure gradient and centrifugal forces) at the Radius of Maximum Winds (RMW), the maximum wind speed is (Holland 1980)

$$W_{max} = \sqrt{B \rho_a^{-1} \exp(-1) \Delta p}. \quad (2.17)$$

Physically, B dictates the shape of the radial pressure profile (Holland 1980, figure 8). Vickery & Wadhera (2009) developed a statistical model for B independent on W_{max} in the form

$$B = 1.881 - 5.57 \times 10^{-6} \text{RMW} - 0.01295 |\psi|, \quad (2.18)$$

where ψ is the latitude (in degrees). In order to use a realistic RMW in comparison to Δp , Vickery & Wadhera (2009)'s relationship for all hurricanes is used

$$\text{RMW} \times 10^{-3} = \exp(3.015 - 6.291 \times 10^{-9} \Delta p^2 + 0.0337 |\psi|). \quad (2.19)$$

Thus for a mid-latitude (45°N) storm, this gives $\text{RMW} \approx 75 \text{ km}$, $B \approx 0.88$ and $W_{max} \approx 41 \text{ m s}^{-1}$. The latter can be reduced to the maximum surface wind $W_{10(max)}$ (1-min average at 10m above the mean sea level) by multiplying by a factor of 0.8 giving $W_{10(max)} \approx 33 \text{ m s}^{-1}$ (Powell 1980). The magnitude of the wind stress can be related to the magnitude of the maximum horizontal wind speed by the conventional bulk formula (e.g. Gill 1982, p. 29): $\tau_0 = c_D \rho_a W_{10(max)}^2$, where c_D is the drag coefficient. The drag coefficient increases as the wind increases for moderate wind speeds ($< 25 \text{ m s}^{-1}$) (Charnock 1955; Smith & Banke 1975; Large & Pond 1981). Although Wu (1982) suggested this increasing relationship was applicable even for wind speeds above hurricane type winds ($> 33 \text{ m s}^{-1}$), several studies showed that c_D levels off or reduces as the wind increases from $\approx 30 \text{ m s}^{-1}$ (Powell *et al.* 2003; Moon *et al.* 2004; Makin 2005; Jarosz *et al.* 2007). Thus an arbitrary value of $c_D = 2.3 \times 10^{-3}$, corresponding to a surface wind of $\approx 33 \text{ m s}^{-1}$, is chosen, consistent with those authors. This gives a maximum wind stress of $\tau_0 \approx 2.9 \text{ Pa}$. The wind direction near the bottom of the atmosphere (i.e. the wind stress direction) can vary from 0° (assuming no stress at the surface of the ocean) to $\text{sgn}(f)45^\circ$

counterclockwise relative to the geostrophic wind direction, as predicted by the Ekman spiral solution for the atmospheric bottom boundary layer (e.g. Garratt 1994, p. 42; Vallis 2006, p. 111), derived from the classical Ekman theory for laminar ocean currents (Ekman 1905). This direction can be arbitrarily chosen without affecting the general model results. For simplicity, let 45° be used. Thus the magnitude of the wind stress components will be taken as $(\tau_0^x, \tau_0^y) = \tau_0 |(\cos, \sin) [\theta - \text{sgn}(f)\pi/4]|$.

2.3. Storm length scale

The estimation of the dominant length scale of storms is poorly documented. It is one of the most relevant parameters of this study. It affects the region forced by the storm, i.e. where there is a significant increase in the surface air entropy, which is always a few times greater than the RMW. Assuming geostrophic balance, the RMW corresponds to the distance between the storm's center and the greatest surface atmospheric pressure gradient. Thus the length scale of a storm is commonly estimated as twice the RMW (e.g. Irish *et al.* 2008). Nevertheless, a more rigorous approach consists of looking at an idealized Gaussian atmospheric pressure profile (in one horizontal dimension) of the form $G = -\exp[-r^2/(2\text{RMW}^2)]$, where r is the distance from the center of the Gaussian. The Fourier transform of the geostrophic wind profile (i.e. the absolute value of the gradient of G) shows that the predominant forcing length scale is $L_g \approx 1.47 \times 2\text{RMW}$ for any RMW.

The geostrophic approach described here is a relatively good approximation for synoptic scale atmospheric systems. However, for mesoscale atmospheric vortices, the gradient wind balance (which has a cyclostrophic balance in the region of maximum winds) is a more realistic assumption. The Fourier transform of (2.16) indicates that the predominant forcing length scale is

$$L = C \times 2\text{RMW}. \quad (2.20)$$

in which $C \approx 1.92$ for $A = 89286^B$, $B = 0.88$ and $\psi = 45^\circ$. The value of A is graphically chosen such that the maximum of the gradient balance wind speed distribution corresponds to $\text{RMW} \approx 75$ km (not shown). Therefore, a storm length scale of $L \approx 288$ km is adopted for the presented examples. Note that, because the gradient wind profile in (2.16) is a function of A , B (or RMW and ψ), Δp and f , the factor C in (2.20) will also depend on those parameters.

2.4. Free wave solutions

Any transient waves reflected by the coast or a topographic step, or transmitted across a step, have free wavelike solutions of the form (e.g. Lamb 1932)

$$\eta_R = \eta_{R0} \exp[i(-k_R x + l_R y - \omega t)], \quad (2.21)$$

$$\eta_T = \eta_{T0} \exp[i(k_T x + l_T y - \omega t)], \quad (2.22)$$

and their respective velocity components have the form:

$$(u_R, v_R) = (u_{R0}, v_{R0}) \exp[i(-k_R x + l_R y - \omega t)], \quad (2.23)$$

$$(u_T, v_T) = (u_{T0}, v_{T0}) \exp[i(k_T x + l_T y - \omega t)], \quad (2.24)$$

which on substitution in (2.5) (without external forcing, $F = 0$) gives the dispersion relation

$$\omega^2 = f^2 + K^2 c^2, \quad (2.25)$$

where $K^2 = K_R^2 = k_R^2 + l_R^2$ and $K^2 = K_T^2 = k_T^2 + l_T^2$ for the reflected and transmitted free waves, respectively. Combining (2.21)-(2.24) and (2.1)-(2.3) (without external forcing)

gives the amplitude of the cross-topography velocity of the transient waves as

$$u_{R0} = \frac{g(-k_R\omega + il_R f)}{\omega^2 - f^2} \eta_{R0}, \quad (2.26)$$

$$u_{T0} = \frac{g(k_T\omega + il_T f)}{\omega^2 - f^2} \eta_{T0}. \quad (2.27)$$

These velocities, with the velocity due to the forced waves (2.13), will be used in the boundary or matching conditions for different topographies.

3. Disturbance crossing a vertical coast

A semi-infinite flat bottom ocean bounded by a vertical coast is considered (figure 1a). Ray theory will be used to determine the wavenumber and angle of the reflected wave (K_R and θ_R , respectively) due to an atmospheric disturbance crossing a vertical coast (figure 1). The forced and reflected waves must have the same frequency ω and alongshore wavenumber ($l_F = l_R = l$) to match their phase structure at the coast (V10). The dispersion relation (2.25) also leads to a relation between the reflected and forced wavenumbers: $K_R = K_F \sqrt{Fr^2 - \tilde{L}^2}$. Thus the relation between the reflected and forced wave angles is

$$\sin \theta_R = \frac{\sin \theta}{\sqrt{Fr^2 - \tilde{L}^2}} = \frac{cK_F \sin \theta}{\sqrt{\omega^2 - f^2}}, \quad (3.1)$$

which can be interpreted as a modified Snell's law of refraction, but applied to reflection of a forced wave (V10). For super-inertial frequency disturbances, a consequence of the modified reflection law is that there is no reflected free wave if θ exceeds the trapped angle

$$\theta_{trap} = \sin^{-1} \left(\sqrt{Fr^2 - \tilde{L}^2} \right) = \sin^{-1} \left[\sqrt{\omega^2 - f^2} / (cK_F) \right], \quad (3.2)$$

which exists only when the disturbance Froude number satisfies

$$\tilde{L}^2 < Fr^2 < 1 + \tilde{L}^2. \quad (3.3)$$

For super-inertial frequency disturbances ($\omega > f$), Fr^2 is always greater than \tilde{L}^2 . If $Fr^2 < 1 + \tilde{L}^2$, then K_R is greater than the radius of the Poincare circle $\sqrt{(\omega^2 - f^2)}/c$ (figure 1b,c). Thus, the transient wave can either be reflected offshore for $|\theta| < \theta_{trap}$ (figure 1b) or trapped along the coast for $|\theta| > \theta_{trap}$ (figure 1c), as the cross-shore wavenumber of the transient wave becomes imaginary: $k_R = i\sqrt{l^2 - (\omega^2 - f^2)}/c$. If $Fr^2 > 1 + \tilde{L}^2$ (fast moving storms), θ_{trap} does not exist but k_R is real, as K_R is smaller than the radius of the Poincare circle. Consequently it will be reflected for all angles (case not shown).

For sub-inertial frequency disturbances ($\omega < f$), Fr^2 is always smaller than \tilde{L}^2 . Therefore (3.3) is violated. The trapped angle, θ_{trap} , and the Poincare circle do not exist and k_R is always imaginary. The reflected wave will always be trapped (figure 1d).

3.1. Coastal solutions

Using (2.13) and (2.26), the solution for the reflected wave (2.21), which satisfies the velocity boundary condition that $u_F + u_R = 0$ at $x = 0$, is

$$\eta_R = \eta_{R0} \exp [i(yK_F \sin \theta - \omega t)] \exp \left\{ \begin{cases} (-ixK_F \sqrt{Fr^2 - \tilde{L}^2 - \sin^2 \theta}) & |\theta| \leq \theta_{trap}, \\ (xK_F \sqrt{\sin^2 \theta + \tilde{L}^2 - Fr^2}) & |\theta| > \theta_{trap}, \end{cases} \right. \quad (3.4)$$

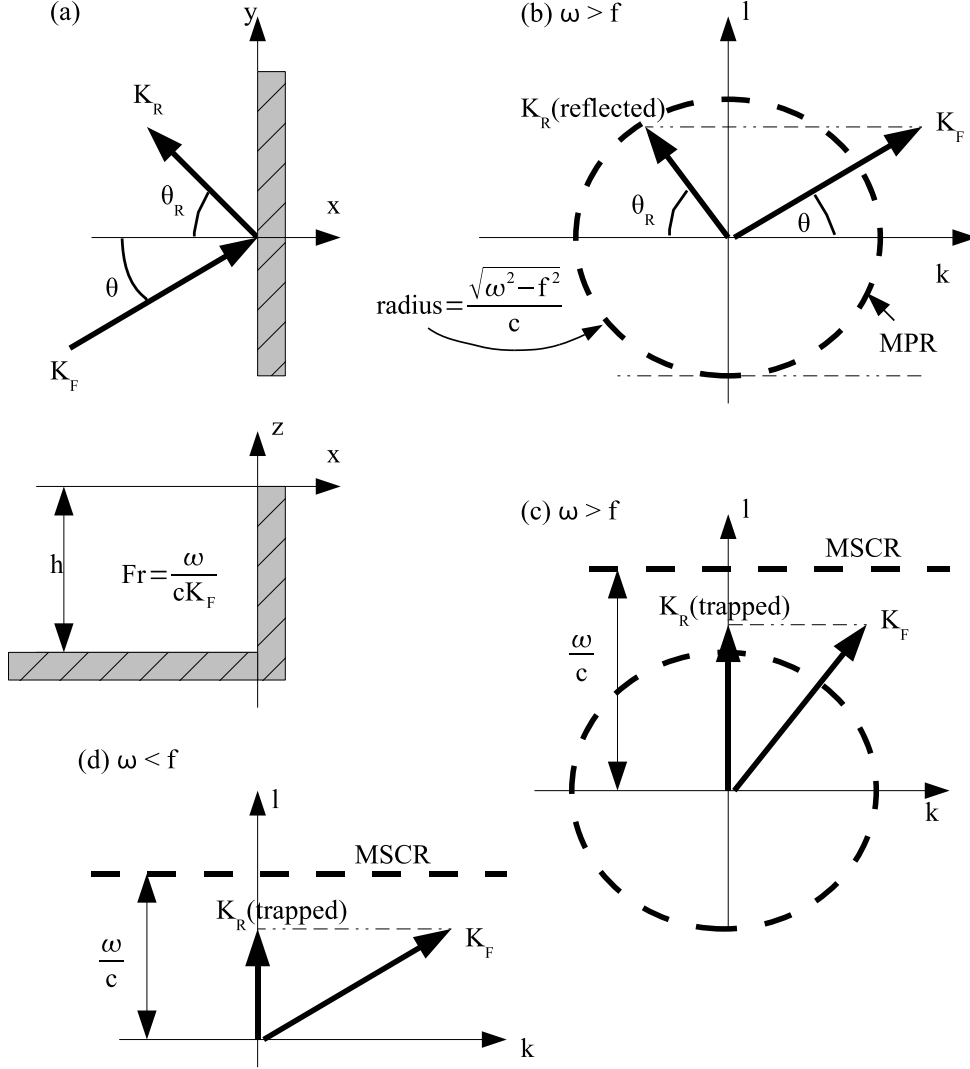


FIGURE 1. (a) Geometry of forced and reflected transient ocean waves due to an atmospheric disturbance crossing a vertical coast with an incident angle θ counterclockwise relative to the x -axis. (b)(c)(d) Dispersion diagrams for the free reflected wave in relation to the forced wave for different cases. Large arrows represent the wavenumber vectors of the forced (K_F) and reflected (K_R) waves. The Poincaré circle is represented in (b) and (c) by a thick dashed lines to illustrate the MPR. Modified Sub-Critical Resonance (MSCR) is represented by an horizontal thick dashed line in (c) and (d).

where

$$\eta_{R0} = \frac{\mathcal{F}}{(1 - Fr^2 + \tilde{L}^2)(k_R\omega - if)}. \quad (3.5)$$

[H]

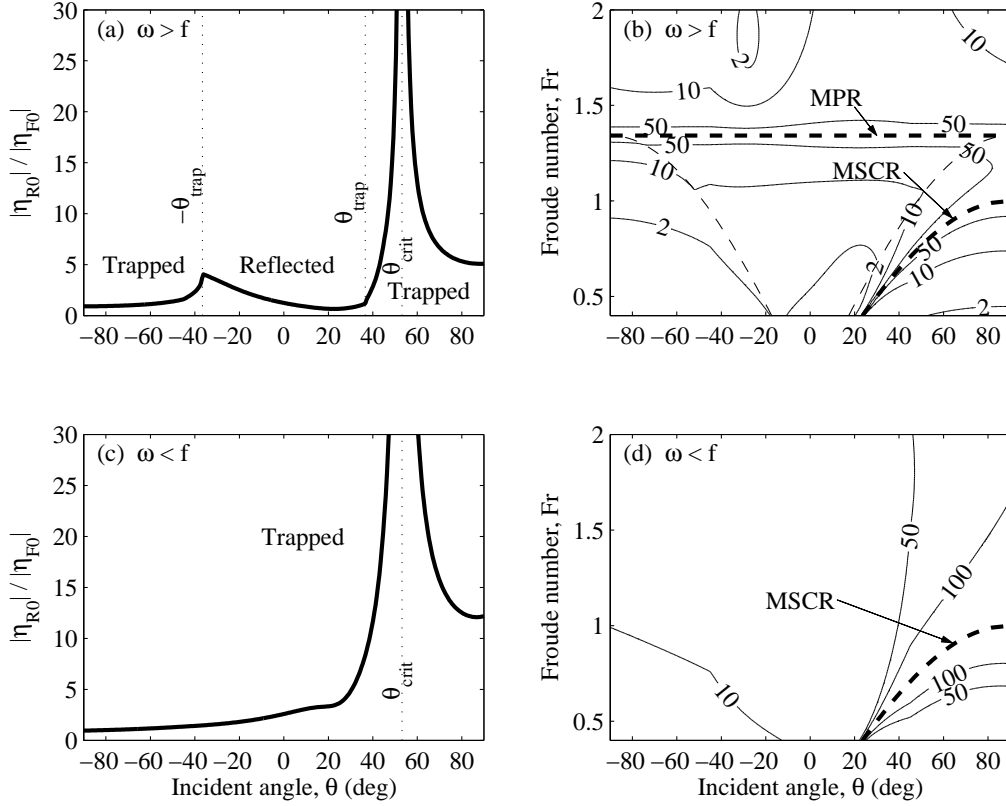


FIGURE 2. (a)(c) Magnitude of the reflected wave $|\eta_{R0}|$ relative to the forced wave $|\eta_{F0}|$ generated by an atmospheric disturbance ($\eta_a = 0.6$ m and $\tau_0 = 2.9$ Pa) crossing a vertical coast for a range of disturbance incident angles and $Fr = 0.8$. (b)(d) Magnitude of $|\eta_{R0}|$ for a range of disturbance incident angles and Froude numbers. The magnitude $|\eta_{R0}|/|\eta_{F0}|$ is contoured instead of $|\eta_{R0}|/|\eta_{F0}|$ in order to show both MPR and MSCR (thick dashed lines). Thin dashed lines in (b) represent $-\theta_{trap}(Fr)$ and $\theta_{trap}(Fr)$. Both cases of (a)(b) super-inertial ($\omega/f = 1.5$) and (c)(d) sub-inertial ($\omega/f = 0.5$) disturbances are considered.

3.2. Resonances

A vanishing denominator in (3.5) gives rise to two types of resonances (figure 2). One is the classic Proudman resonance (Lamb 1932; Proudman 1953) modified by rotation. In order to generate this Modified Proudman Resonance (MPR), the resonant Froude number Fr^{res} must be greater than unity: $Fr^{res} = \sqrt{1 + \tilde{L}^2}$. Thus, because of the Earth's rotation, the larger the storm is compared to the depth, the faster it has to travel to generate MPR. Graphically this kind of resonance occurs when the disturbance's wavenumber K_F matches the radius of the Poincare circle $\sqrt{(\omega^2 - f^2)}/c$ (figure 1b,c). Therefore Fr^{res} can be expressed in terms of frequencies as $Fr^{res} = (1 - f^2/\omega^2)^{-1/2}$. Note that MPR cannot occur for sub-inertial disturbances (figures 1d and 2d).

The second kind of resonance occurs only for complex imaginary k_R (i.e. only if the reflected transient is trapped at the coast) and can be interpreted as sub-critical resonance (V10) modified by rotation. It occurs only if $l^2 > (\omega^2 - f^2)/c^2$. The critical cross-shore wavenumber k_{Rcrit} in (3.5), for which η_{R0} tends to infinity, is

$$k_{Rcrit} = i l_{crit} f / \omega, \quad (3.6)$$

where l_{crit} is the corresponding critical along-shore wavenumber defined by $\sin \theta_{crit} = l_{crit}/K_F$. From the dispersion relation (2.25) when $l^2 > (\omega^2 - f^2)/c^2$, we can write:

$$k_{Rcrit} = \pm i \sqrt{l_{crit}^2 - (\omega^2 - f^2)/c^2}. \quad (3.7)$$

Combining (3.6) and (3.7), we find $l_{crit} = \pm \omega/c$. If $l_{crit} = -\omega/c$ then $k_{Rcrit} = -iL_r^{-1}$ and the form of the reflected wave, $\eta_R = \eta_{R0} \exp(-L_r^{-1}x) \exp[i(l y - \omega t)]$, would grow as $x \rightarrow -\infty$ (towards deep water), which is not geometrically possible. Therefore, the only alongshore wave number that generates Modified Sub-Critical Resonance (MSCR) in the Northern Hemisphere is $l_{crit} = \omega/c$. This means that the alongshore component of the forcing wavenumber must have the coast on the right (i.e. right-bounded disturbances). Consequently, the trapped wave also propagates with the coastline on its right in the Northern Hemisphere. The corresponding critical angle is

$$\theta_{crit} = \sin^{-1}(Fr), \quad (3.8)$$

which is the same as the critical angle for sub-critical resonance without rotation (V10). Note that the critical angle in the Southern Hemisphere is $\theta = \sin^{-1}(-Fr)$ due to the negative sign of f in (3.6). This resonance is similar to the sub-critical resonance given by V10 in the sense that it can only occur for sub-critical storms impacting the coast at a specific angle (figure 2). However, using a more general approach considering Coriolis effects, it is shown here that MSCR can occur only when the transient is trapped, i.e. $\theta_{crit} > \theta_{trap}$ (figures 1 and 2) ($\theta_{crit} = \theta_{trap}$ in V10).

Considering the case of a sub-inertial disturbance ($\omega < f$, figure 2c,d), although MPR does not exist, MSCR can occur and large response is spread over a wider range of incident angles around θ_{crit} (figure 2c) compared to the super-inertial case (figure 2a). The wavenumber components k_{Rcrit} and l_{crit} correspond to the well-known Kelvin-wave solution (e.g. Longuet-Higgins 1968a; Thomson 1970). Resonance occurs when the along-shore phase speed of the forced wave (ω/l) matches the free Kelvin-wave phase speed (\sqrt{gh}).

Theory predicts infinite sea level elevation at resonance. Nevertheless, because of non-linearity and frictional effects, complete resonance cannot occur in a real ocean. Therefore resonance must be interpreted as a strong amplification instead of infinite rise of sea level.

Note that the choice of the forcing values in \mathcal{F} (i.e. $\eta_{a0}, \tau_0^x, \tau_0^y$ in section 3) only influences the amplitude of the transient and forced waves, not the structure of the resonances inherent in (3.5). Thus the forcing can be chosen arbitrarily, as it only slightly affects the ratio $|\eta_{R0}(Fr, \theta)|/|\eta_{F0}(Fr, \theta)|$, but without any changes to the critical resonant angles (figure 2a,c).

4. Disturbance crossing a step

An infinite rotating ocean with a step at $x = 0$ and uniform depths on both sides is considered (figure 3a). Both a reflected and a transmitted transient free wave are generated when an atmospherically forced wave crosses a step (figure 3). Using ray theory, the frequency and the wavenumber parallel to the step of the two transients waves must match those of the forced wave, i.e. $l_R = l_T = l_F = l$. Equation (2.25) shows that

$$K_R = K_F \sqrt{Fr_d^2 - \tilde{L}_d^2} \quad \text{and} \quad K_T = K_F \sqrt{Fr_s^2 - \tilde{L}_s^2}, \quad (4.1)$$

where $Fr_d = \omega/(c_d K_F)$ and $\tilde{L}_d = f/(c_d K_F)$ are the forcing Froude number and dimensionless disturbance width, respectively, on the deep side of the step. The subscripts d

and s indicate the deep and shallow sides of the step hereafter. Following V10 but taking into account the Earth's rotation, the modified Snell's law applied to the deep and shallow sides of the step are

$$\sin \theta_R = \frac{\sin \theta}{\sqrt{Fr_d^2 - \tilde{L}_d^2}} = \frac{c_d K_F \sin \theta}{\sqrt{\omega^2 - f^2}} \quad \text{and} \quad (4.2)$$

$$\sin \theta_T = \frac{\sin \theta}{\sqrt{Fr_s^2 - \tilde{L}_s^2}} = \frac{c_s K_F \sin \theta}{\sqrt{\omega^2 - f^2}}, \quad (4.3)$$

respectively, which gives different trapped angles for the reflected and transmitted waves:

$$\theta_{trapR} = \sin^{-1}(\sqrt{Fr_d^2 - \tilde{L}_d^2}) = \sin^{-1} \left[\sqrt{\omega^2 - f^2} / (c_d K_F) \right] \quad \text{and} \quad (4.4)$$

$$\theta_{trapT} = \sin^{-1}(\sqrt{Fr_s^2 - \tilde{L}_s^2}) = \sin^{-1} \left[\sqrt{\omega^2 - f^2} / (c_s K_F) \right]. \quad (4.5)$$

Again, (4.4) and (4.5) show that θ_{trapR} and θ_{trapT} exist only for super-inertial disturbances if $\tilde{L}_d^2 < Fr_d^2 < 1 + \tilde{L}_d^2$ and $\tilde{L}_s^2 < Fr_s^2 < 1 + \tilde{L}_s^2$, respectively. If the forcing frequency is lower than the inertial frequency f , the reflected and transmitted transient waves will always be trapped along the discontinuity in depth.

4.1. Interpretation of the dispersion diagram

A detailed interpretation of the various cases can be made using the dispersion diagram of figure 3. For super-inertial disturbances, $\omega > f$, three cases are considered. Firstly, if $|\theta| < \theta_{trapR}$, the transients will be reflected and transmitted on both sides of the step without trapping (figure 3b). Secondly, if $\theta_{trapR} < \theta < \theta_{trapT}$, the transients will be trapped on the deep side and transmitted on the shallow side (figure 3c). Finally, if $\theta > \theta_{trapT}$ (figure 3d) trapping will occur on both sides of the discontinuity and can be interpreted as a 'forced' double Kelvin wave.

For sub-inertial disturbances, $\omega < f$ (figure 3e), both transient waves will be trapped for any incident angle. The Poincare semi-circles are represented in figure 3b-d to show the radius changes on either side of the step and the MPR, which is assumed to occur only on the shallow side. Sub-inertial resonance is represented by a thick dashed line in figure 3e.

As in section 3, the case when $Fr_s^2 > 1 + \tilde{L}_s^2$ is omitted because here we are not concerned with very fast moving storms.

4.2. Step solutions

The reflected and transmitted waves, η_R and η_T respectively, can be expressed in terms of the wavenumber K_F and the incident angle θ of the forcing as

$$\eta_R = \eta_{R0} \exp [i (y K_F \sin \theta - \omega t)] \exp \begin{cases} (-i K_F \alpha_d x) & |\theta| \leq \theta_{trapR}, \\ (K_F \alpha_d^* x) & |\theta| > \theta_{trapR}, \end{cases} \quad (4.6)$$

$$\eta_T = \eta_{T0} \exp [i (y K_F \sin \theta - \omega t)] \exp \begin{cases} (i K_F \alpha_s x) & |\theta| \leq \theta_{trapT}, \\ (-K_F \alpha_s^* x) & |\theta| > \theta_{trapT}, \end{cases} \quad (4.7)$$

where $\alpha_d = \sqrt{Fr_d^2 - \tilde{L}_d^2 - \sin^2 \theta}$ and $\alpha_d^* = \sqrt{\sin^2 \theta + \tilde{L}_d^2 - Fr_d^2}$.

Matching the elevation and mass transport, at $x = 0$, of the forced and reflected waves on the deep side of the step with the transmitted and enhanced forced waves on the

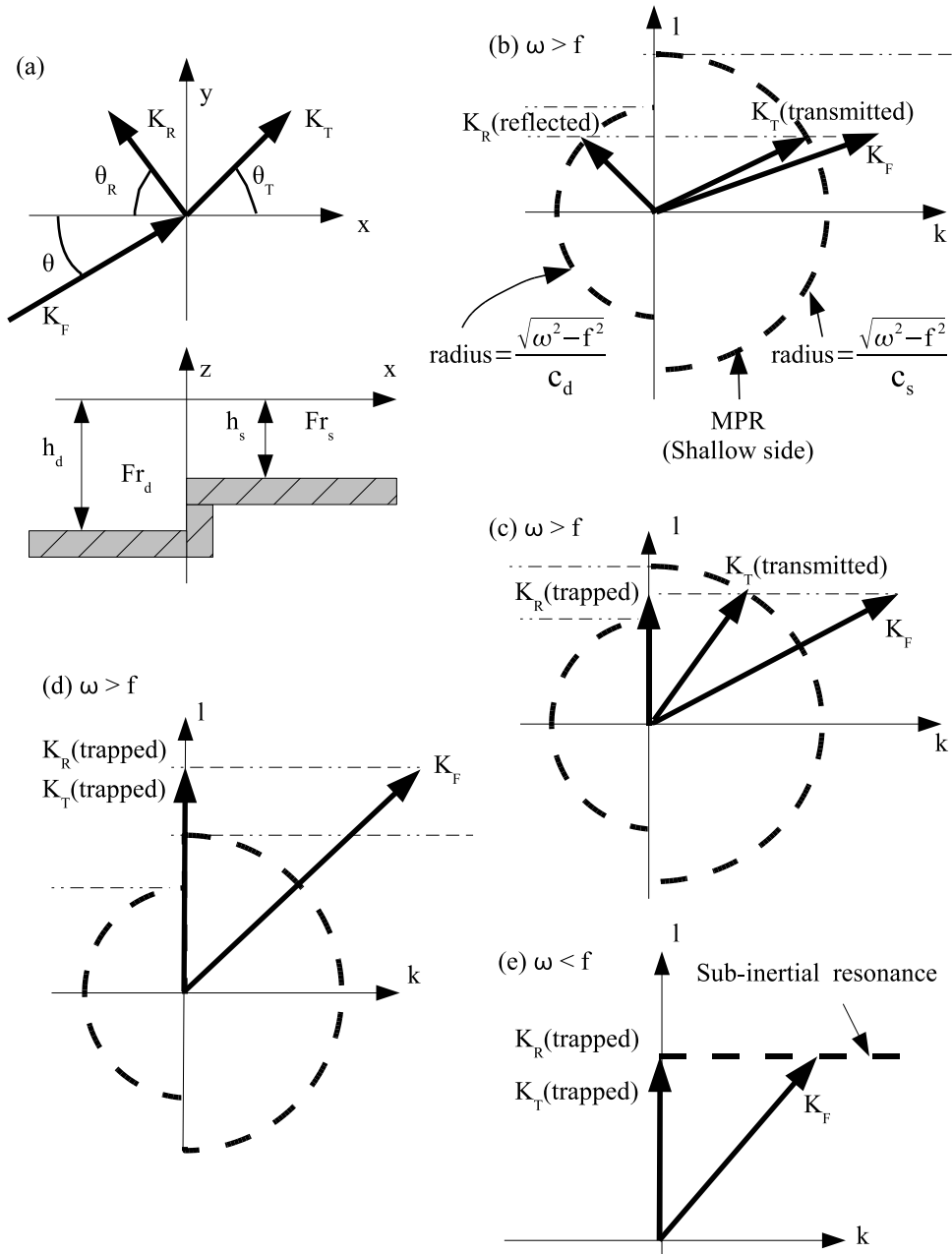


FIGURE 3. (a) Geometry of the step in the (x,y) and the (x,z) planes. (b)(c)(d)(e) Dispersion diagrams for the free transient waves and relation to the forced wave for different cases. Large arrows represent the wavenumber vectors of the forced (K_F), reflected (K_R) and transmitted (K_T) waves. The Poincare semi-circles in (b), (c) and (d) and sub-inertial resonance in (e) are represented by thick dashed lines.

shallow side gives the reflection and transmission coefficients as the amplitudes of

$$\eta_{R0} = [\gamma \mathcal{F}_d M_s - \mathcal{F}_s M_d + (M_d F_{0s} - M_s F_{0d})(ilf + k_T \omega)] / (\Delta M_d M_s), \quad (4.8)$$

$$\eta_{T0} = [\gamma \mathcal{F}_d M_s - \mathcal{F}_s M_d + \gamma (M_d F_{0s} - M_s F_{0d})(ilf - k_R \omega)] / (\Delta M_d M_s), \quad (4.9)$$

where $\gamma = h_d/h_s = (Fr_s/Fr_d)^2 > 1$, $M_d = 1 - Fr_d^2 + \tilde{L}_d^2$, $M_s = 1 - Fr_s^2 + \tilde{L}_s^2$ and

$$\Delta = [\omega(\gamma k_R + k_T) - ilf(\gamma - 1)]. \quad (4.10)$$

The structure of (4.8) and (4.9) shows that there are three ways to generate resonance, i.e. when either M_d , M_s or Δ vanishes.

It will be demonstrated that two kinds of resonance can occur when a disturbance obliquely crosses a discontinuity in depth and that they are mutually exclusive. One can only occur for super-inertial disturbances and the other for sub-inertial disturbances. Thus it is not possible to visualize them in a unique graph and so they must be treated separately.

4.3. Modified Proudman resonance: $M_d = 0$ or $M_s = 0$

Considering a storm moving over deep water in a real ocean, M_d is unlikely to vanish because an extremely fast disturbance speed is needed to obtain a Froude number approaching $Fr^{res} = (1 - f^2/\omega^2)^{-1/2}$ to give MPR in deep water. If M_s vanishes, then MPR occurs when a super-inertial disturbance crosses a step for a specific resonant shallow water Froude number Fr^{res} greater than 1 (figure 4b). The classic Proudman resonance occurs at the step for fast moving storms in a non-rotating ocean when $Fr_s \approx 1$ for all incident angles enhancing the transmitted wave amplitude. V10 showed that the reflected wave amplitude is almost zero for all incident angles and Fr_s . Here for a rotating ocean, super-inertial disturbances conceptually give similar results (figure 4a,b), but for $Fr_s = Fr^{res} > 1$ instead of $Fr_s \approx 1$.

4.4. Sub-inertial resonance: $\Delta = 0$

As (4.10) is complex, this resonance can occur only when both k_R and k_T are complex and figure 4 shows that the frequency must be sub-inertial ($\omega < f$). Sub-inertial disturbances can generate a new kind of resonance which magnifies both transmitted and reflected waves at a critical incident angle θ_{Scrit} (figure 4c,d).

We can write Δ in (4.10) in terms of θ and K_F as

$$\Delta = iK_F \left[\omega \left(\gamma \sqrt{\sin^2 \theta + \tilde{L}_d^2 - Fr_d^2} + \sqrt{\sin^2 \theta + \tilde{L}_s^2 - Fr_s^2} \right) - f(\gamma - 1) \sin \theta \right]. \quad (4.11)$$

Thus there exists a critical angle θ_{Scrit} for which Δ vanishes. It is possible to determine θ_{Scrit} numerically but it can also be found by the intersection of two curves described in sub-section 4.5. The next sub-section explores the dispersion relation of double Kelvin waves (DKWs) which are linked to this sub-inertial resonance.

4.5. Sub-inertial resonance and double Kelvin waves.

Longuet-Higgins (1968a) showed theoretically the existence of DKWs trapped along a discontinuity of depth in a rotating ocean. These types of motion exist only at sub-inertial frequencies and always travel in the direction of Kelvin waves in the deeper fluid, i.e. having the shallower water to their right in the Northern Hemisphere. Their phase speed is always greater than the corresponding Kelvin-wave phase speed (on the deeper side) to which they may tend whenever $f^2/(mc_d)^2 > 1$ (where m is the along-step component of the free DKW wavenumber) (Longuet-Higgins 1968a).

[H]

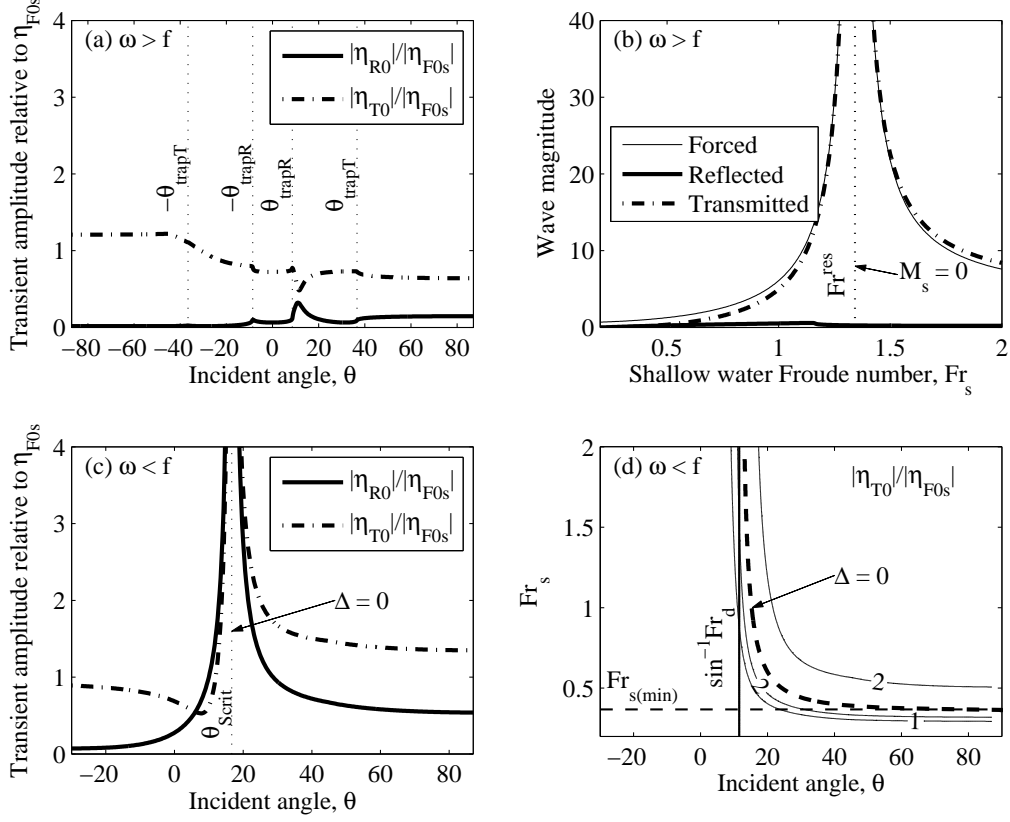


FIGURE 4. (a)(c) Magnitude of the reflected, $|\eta_{R0}|$, and transmitted, $|\eta_{T0}|$, free waves relative to the shallow water forced wave $|\eta_{F0s}|$ under a (a) super- ($\omega/f = 1.5$) and (c) sub-inertial ($\omega/f = 0.5$) disturbance crossing a step for a range of disturbance incident angles, $Fr_d = 0.2$ and $Fr_s = 0.8$. (b) Magnitude of $|\eta_{F0s}|$, $|\eta_{R0}|$ and $|\eta_{T0}|$ generated by a super-inertial ($\omega/f = 1.5$) disturbance crossing a step for a range of shallow water Froude numbers, $Fr_d = 0.2$ and $\theta = 60^\circ$. (d) Magnitude of $|\eta_{T0}|$ relative to $|\eta_{F0s}|$ under a sub-inertial ($\omega/f = 0.5$) atmospheric disturbance crossing a step for $Fr_d = 0.2$ and a range of disturbance incident angles and shallow water Froude numbers. The thick dashed line represents sub-inertial resonance.

The incident angle $\theta_{dk} = \sin^{-1}(m/K_F)$ corresponding to m for a given wavenumber forcing K_F can be found by the intersection of the two families of curves:

$$F(\gamma, \sigma, \theta, f) = -\gamma^{-\frac{1}{2}} K_F \sin \theta_{dk} \sqrt{f^2/\sigma^2 - 1}, \quad (4.12)$$

$$G(c_d, \sigma, \theta, f) = K_F \sin \theta_{dk} \left(\sqrt{1 + (f^2 - \sigma^2)/(c_d K_F \sin \theta_{dk})^2} - f/\sigma \right), \quad (4.13)$$

where σ denotes the angular frequency of the free DKW. Equations 4.12 and 4.13 are the relations found by Longuet-Higgins (1968a, equations (3.23) and (3.24)) generalized for any $f > 0$ and m and reinterpreted for the geometry of figure 3a. This gives the incident angle:

$$\theta_{dk} = \sin^{-1} \left(Fr_d \sqrt{\frac{f^2/\sigma^2 - 1}{\left(f/\sigma - \gamma^{-\frac{1}{2}} \sqrt{f^2/\sigma^2 - 1} \right)^2 - 1}} \right), \quad (4.14)$$

which is the same as the critical angle θ_{Scrit} in (4.11) for which Δ vanishes when $\sigma = \omega$ (figure 4d). This study shows that resonance can occur at a discontinuity in depth when the along-step component of the phase speed of the forced wave (ω/l) matches the double Kelvin-wave phase speed (σ/m).

Note that if $h_d \gg h_s$, the critical angle of resonance tends to $\sin^{-1}(Fr_d)$ (figure 4d) as in section 3 for a vertical coast. From figure 4d, note that there is minimum shallow water Froude number under which no resonance can occur for any θ . In fact there is a minimum γ , which can be written from (4.14) when $\theta_{dk} \rightarrow \pi/2$, as

$$\gamma_{min} = (f^2/\omega^2 - 1) \left(\sqrt{Fr_d^2 (f^2/\omega^2 - 1) + 1} - f/\omega \right)^{-2}. \quad (4.15)$$

Thus for a given h_s , the depth on the deep side must be greater than $h_d = h_s \gamma_{min}$ (i.e. the shallow water Froude number must be greater than $Fr_{s(min)} = Fr_d \sqrt{\gamma_{min}}$, figure 4d) for resonance to be possible. In other words, sub-inertial resonance can only occur for sufficiently large steps.

5. Disturbance crossing a continental shelf

An idealized step-shelf topography is considered (figure 5). As the disturbance crosses the shelf break ($x = 0$), a transient free wave, $R1$, is reflected back into deep water and a larger free wave, T , is transmitted onto the shelf. The transient wave T is then reflected at the coast and either reflected or partly transmitted (by leakage) into the deeper side at the shelf break (figure 5b) (V10). In a rotating ocean, super-inertial free waves crossing a step from the shallower side will be totally reflected if the incident angle exceeds $\sin^{-1}(c_s/c_d)$, which is independent of the Coriolis parameter (Longuet-Higgins 1968a). LeBlond & Mysak (1978) gave the same angle for total reflection at a step in a non-rotating ocean. Thus T is totally reflected at the step and consequently trapped on the shelf if the incident angle of the forcing exceeds the critical angle $|\theta| = \theta_{trapR}$.

If $|\theta| < \theta_{trapR}$, then the transient waves, after being reflected at the coast, will be at least partially transmitted (leaked) to deep water at the shelf break (figure 5b) (Longuet-Higgins 1968a; V10). The transmitted wave T is internally reflected over the shelf for $\theta_{trapR} < |\theta| < \theta_{trapT}$ and acts as a forced Poincare wave trapped on the shelf which can be a source of excitation of edge wave modes. For $\theta > \theta_{trapT}$, T is trapped and forms an exponentially decaying wave on the shelf, acting as a ‘Forced Kelvin wave’ on the shallow side of the shelf break.

A free reflected wave, $R2$, is also generated when the disturbance crosses the coast ($x = W$) and will have the same direction as the transient T after reflection from the coast. Thus, the transient $R2$ will have the same fate as T depending on the incident angle of the disturbance. However, as commented on by V10, the standing wave form of $R2$ can exchange water with the trapped decaying exponential wave in deep water. Hence $R2$ cannot generate resonant conditions at the step in a non-rotating ocean (V10), and will not be discussed here.

5.1. Shelf solutions

The amplitude reflection coefficient of a reflected plane Poincare wave against a vertical coast (at $x = W$) is written in the form (LeBlond & Mysak 1978, p. 199): $R_p = (\omega k_T + ifl)/(\omega k_T - ifl)$. Thus a trapped transient T over the shelf may be written as a superposition of two plane Poincare waves as (LeBlond & Mysak 1978):

$$\eta_T = \eta'_{T0} \cos[k_T(x - W) - \phi_{k_T}] \exp[i(l y - \omega t)], \quad (5.1)$$

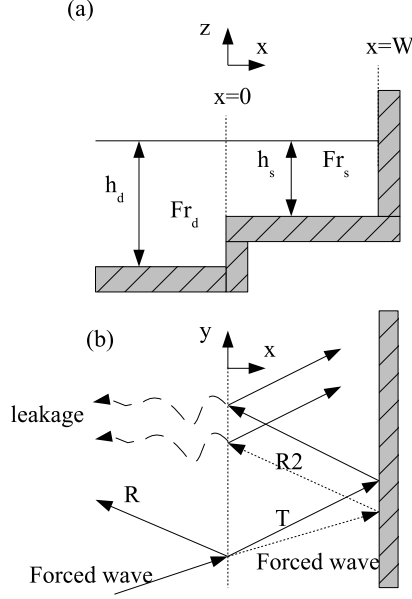


FIGURE 5. (a) Idealized topography of the step shelf. (b) Schematic ray paths for the transients generated by an atmospheric disturbance crossing the continental shelf. Only the case $\theta < \theta_{trapR}$ is shown, but the transients R and $R2$ are trapped if $\theta > \theta_{trapR}$ as well as T if $\theta > \theta_{trapT}$. When $\theta > \theta_{trapR}$, no leakage occurs.

where $\phi_{k_T} = \arg(\omega k_T + i f l) = \tan^{-1}[f l / (\omega k_T)]$. As a consequence of the sinusoidal structure of the transient response in 5.1 (which becomes an hyperbolic-sinusoidal structure for trapped transients), the transient amplitude (i.e. $\eta'_{T0} \cos[k_T(x - W) - \phi_{k_T}]$ in (5.1)) is a function of x across the shelf. Thus the form of the transmitted transient can be written

$$\eta_T = \eta_{T0}(x) \exp[i(l y - \omega t)], \quad (5.2)$$

where, within the interval $x = [0, W]$,

$$\eta_{T0}(x) = \eta'_{T0} \begin{cases} \cos[K_F \alpha_s(x - W) - \phi] & |\theta| < \theta_{trapT}, \\ \cosh[K_F \alpha_s^*(x - W) - \phi^*] & |\theta| \geq \theta_{trapT}, \end{cases} \quad (5.3)$$

in which $\phi = \tan^{-1}[f \sin \theta / (\alpha_s \omega)]$ and $\phi^* = \tanh^{-1}[-f \sin \theta / (\alpha_s^* \omega)]$. Figure 6 shows the shape of four different trapped free wave modes that can resonate with the forced wave depending on frequency and incident angle of the disturbance and the shelf width.

By combining (5.1) and (2.1)-(2.2), the component of cross-shore velocity on the shelf has the form

$$u_T = g \eta'_{T0} i \frac{k_T \omega \sin[k_T(x - W)]}{(\omega^2 - f^2) \cos \phi_{k_T}} \exp[i(l y - \omega t)], \quad (5.4)$$

which can be written in terms of K_F and θ as:

$$u_T = i g \eta'_{T0} \omega K_F \exp[i(K_F \sin \theta y - \omega t)] \begin{cases} \alpha_s \frac{\sin[K_F \alpha_s(x - W)]}{(\omega^2 - f^2) \cos \phi} & |\theta| < \theta_{trapT}, \\ \alpha_s^* \frac{\sinh[-K_F \alpha_s^*(x - W)]}{(\omega^2 - f^2) \cosh \phi^*} & |\theta| \geq \theta_{trapT}. \end{cases} \quad (5.5)$$

Matching the elevation and mass transport at the step, $x = 0$, of the reflected wave

[H]

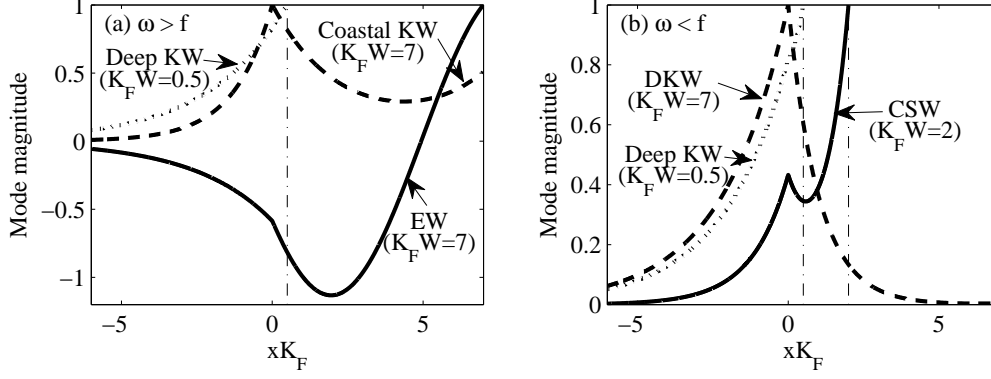


FIGURE 6. Shape of the wave modes that can be excited on the shelf by (a) super-inertial and (b) sub-inertial disturbance for different dimensionless shelf widths $K_F W$. EW = edge wave; KW = Kelvin wave; DKW = double Kelvin wave; CSW = continental shelf wave. The vertical dash-dot lines represent the coastline (at $x = W$) when (a) $K_F W = 0.5$ and (b) $K_F W = 2$; when $K_F W = 7$, the coastline is on the right edge of the graphs.

and the deep water forced wave with this transmitted wave and the enhanced forced wave over the shelf gives the transmission coefficient as the amplitude of

$$\eta_{T0}(x) = \frac{[\gamma \mathcal{F}_d M_s - \mathcal{F}_s M_d + \gamma (M_d F_{0s} - M_s F_{0d}) (ilf - k_R \omega)]}{\Delta_{sh}(x) M_d M_s}, \quad (5.6)$$

where

$$\Delta_{sh}(x) = \left[-i\omega k_T \frac{\sin(k_T W)}{\cos \phi_{k_T}} + \gamma (k_R \omega - ilf) \cos(k_T W + \phi_{k_T}) \right] \{ \cos[k_T(x - W) + \phi_{k_T}] \}^{-1}. \quad (5.7)$$

Modified Proudman resonance can occur for a specific shallow water Froude number and super-inertial disturbances but, again, the amplitude of the transmitted transient wave is comparable to the amplitude of the enhanced forced wave on the shelf, similar to figure 4b for a step.

As we are interested in storm surges, we shall express $\Delta_{sh}(x)$ in terms of K_F and θ at the coast, $x = W$, as:

$$\Delta_{sh[x=W]} = K_F \begin{cases} i\omega \alpha_s \frac{\sin(-K_F \alpha_s W)}{\cos^2 \phi} + \gamma (\alpha_d \omega - if \sin \theta) \frac{\cos(K_F \alpha_s W + \phi)}{\cos \phi} & |\theta| \leq \theta_{trapR}, \\ i\omega \alpha_s \frac{\sin(-K_F \alpha_s W)}{\cos^2 \phi} + i\gamma (\alpha_d^* \omega - f \sin \theta) \frac{\cos(K_F \alpha_s W + \phi)}{\cos \phi} & \theta_{trapR} < |\theta| < \theta_{trapT}, \\ i\omega \alpha_s^* \frac{\sinh(K_F \alpha_s^* W)}{\cosh^2 \phi^*} + i\gamma (\alpha_d^* \omega - f \sin \theta) \frac{\cosh(K_F \alpha_s^* W + \phi^*)}{\cosh \phi^*} & |\theta| \geq \theta_{trapT}. \end{cases} \quad (5.8)$$

Figure 7 shows the magnitude of the transmitted wave relative to the forced wave crossing a step shelf for a range of nondimensional shelf widths, $K_F W$, and incident angles in order to show the possible wave mode excitations for super- and sub-inertial disturbances for three different Fr_s .

5.2. Edge wave resonance at the coast

For super-inertial disturbances (figure 7a-c), edge-wave modes (with frequencies greater than f) can be excited if $\theta_{trapR} < |\theta| < \theta_{trapT}$ when the phase speed of the disturbance along the coast matches the alongshore phase speed of one of the infinite discrete set of

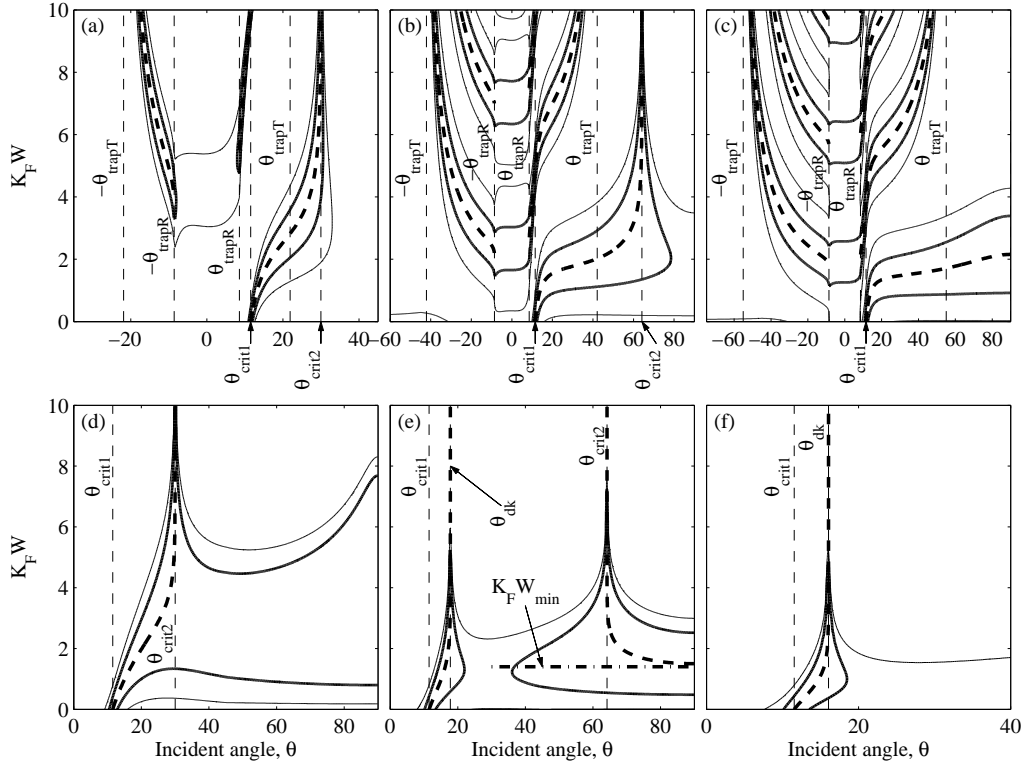


FIGURE 7. Amplitude of transmitted wave transient $|\eta_{T0}|$, (5.2), relative to the amplitude of the forced wave $|\eta_{F0s}|$, (2.8), at the coast, $x = W$, as a function of dimensionless shelf width and incident angle for $Fr_d = 0.2$ and (a)(d) $Fr_s = 0.5$, (b)(e) $Fr_s = 0.9$ and (c)(f) $Fr_s = 1.1$ considering a (a)(b)(c) super- and (d)(e)(f) sub-inertial disturbance crossing a step shelf. Thick dashed lines indicate the edge / Kelvin / double Kelvin / shelf wave mode excitations. Contour levels of 1 and 2 are represented by thin and thick solid lines, respectively. Trapped and critical incident angles are shown by thin vertical dashed lines. The thick horizontal dot-dashed line in (e) represents the minimum dimensionless shelf width $K_F W_{min}$ for shelf wave excitation.

edge waves (propagating with the coast either on the right or left) (Munk *et al.* 1970; Huthnance 1975; Johns & Lighthill 1993; Lighthill 1998). The transmitted wave response for positive and negative incident angles is asymmetric because of the Earth's rotation. V10 showed only the transient responses for positive angles because Coriolis effects were neglected and thus the responses were symmetric.

5.3. KW resonance at the coast

Figure 7a,b,d,e shows that resonance occurs on a wide shelf for the critical angle $\theta_{crit2} = \sin^{-1}(Fr_s)$, which corresponds to the critical angle found in section 3 for the vertical coast. Note that, on a wide shelf, the KW amplitude at the coast is relatively small for sub-inertial disturbances (figure 6b) and resonance may be weakened. For the special case of $K_F W = 0$ (i.e. no shelf) the critical angle becomes $\theta_{crit1} = \sin^{-1}(Fr_d)$.

A unique KW mode can be excited if $\theta_{crit1} < \theta < \theta_{crit2}$ when its alongshore phase speed corresponds to the phase speed of the disturbance along the coast, propagating with the coastline on its right (left) in the Northern (Southern) Hemisphere. At high frequencies and alongshore phase speeds (i.e. small incident angles), it becomes a right-bounded fundamental-mode edge wave (Huthnance 1975; Mysak 1980).

For both sub- and super-inertial sub-critical disturbances moving over wide shelves (figure 7a,b,d,e), the angle θ_{crit2} is responsible for the Kelvin wave mode excitation. For super-critical speed disturbances in shallow water (figure 7c,f), this angle does not exist at either super- or sub-inertial frequencies, which means that, again, the Kelvin mode becomes a right-bounded fundamental-mode edge wave (Huthnance 1975; Mysak 1980) for super-inertial disturbances with θ between θ_{crit1} and 90° (figure 7c). In this case, the KW mode disappears for sub-inertial disturbances (figure 7f).

5.4. DKW resonance at the shelf break

For sub-inertial disturbances (figure 7e,f), a single double Kelvin wave mode can be excited only for disturbances with positive (negative) alongshore wavenumbers in the Northern (Southern) Hemisphere. For the DKW mode, several limiting cases are of interest. Firstly, when $K_F W \rightarrow 0$ (i.e. no shelf), figure 7e,f shows that the critical angle for DKW mode excitation tends to $\theta_{crit1} = \sin^{-1} Fr_d$, consistent with the results for a vertical coast (section 3). Secondly, as in section 4 for a step, the DKW mode cannot be excited for shallow water Froude number smaller than $Fr_{s(min)} = Fr_d \sqrt{\gamma_{min}}$ (figure 7d). Thirdly, for relatively wide shelves, the solution for η_T (5.1) should exhibit exponential decay (as in section 4) rather than sinusoidal behavior. Thus the unique angle of excitation becomes $\theta \approx \theta_{dk}$ of (4.14) (step case). Finally, for very wide shelves (upper part of figure 7e,f), the trapped transient generated at the step, responsible for the possible DKW excitation if $\omega < f$, is enhanced only for an extremely narrow angle range, which indicates that mode excitation is less likely to occur. Furthermore, the trapped transient amplitude (decaying exponentially on both sides of the step) is too small at the coast to possibly excite the KW mode, for both super- and sub-inertial frequencies. Note that the narrowing of the DKW mode excitation for wide shelves is due to the fact that we presented only the transmitted wave amplitude at the coast, $x = W$. Considering the response at the step, $x = 0$, the DKW mode can be excited for any shelf width and this shows similar results (not shown) to section 4. In other words, although the exponential decaying transient it is not ‘felt’ at the coast for wide shelves, resonance can still occur at the shelf break (figure 6b).

It should be noted that if $Fr_s < Fr_{s(min)} = Fr_d \sqrt{\gamma_{min}}$, the DKW mode cannot exist at sub-inertial frequencies (as θ_{dk} does not exist) but is replaced by the Kelvin mode which occurs for $\theta_{crit1} \leq \theta < \theta_{crit2}$ (figure 7d).

5.5. The shelf wave resonance

On a step shelf, only the first mode shelf wave can be excited (Larsen 1969; Munk *et al.* 1970; Huthnance 1975). It can be excited when $\theta > \theta_{crit2}$ for relatively narrow shelves only for right (left) bounded forced waves in the Northern (Southern) Hemisphere (figure 7e). Only frequencies smaller than

$$\omega_{maxSh} = f(\gamma - 1)/(\gamma + 1) \quad (5.9)$$

can excite this mode for large angles of incidence (figure 7e) (Munk *et al.* 1970, figure 6 and equation (31)). Disturbances with frequency greater than ω_{maxSh} will excite the KW mode for small incident angles between $\theta_{crit1} \leq \theta < \theta_{crit2}$ (not shown), similar to the previous remark for low Fr_s (sub-section 5.4). Following Munk *et al.* (1970, equation (30)), for small l (bottom part of figure 7e), the shelf wave dispersion relation for a step shelf of width W becomes

$$\sigma_{sh} \approx f \lambda l_{sh} (1 - \gamma^{-1}) \gamma^{-1/2} \tanh(\gamma^{1/2} W \lambda^{-1}), \quad (5.10)$$

where $\lambda = c_d/f$ is the ‘inertial length’, σ_{sh} and l_{sh} are the frequency and alongshore

wavenumber of the ‘free’ shelf wave, respectively. The shelf wave alongshore phase speed, σ_{sh}/l_{sh} , decreases as W reduces. Therefore, the alongshore phase speed of the forced wave, $\omega/(K_F \sin \theta)$, must decrease (i.e. the incident angle θ must increase) to excite the shelf wave mode (bottom-right part of figure 7e). Furthermore, the minimum shelf width under which no shelf mode can be excited can be approximated when $\theta \rightarrow 90^\circ$ by

$$K_F W_{min} \approx \frac{\lambda K_F}{\sqrt{\gamma}} \tanh^{-1} \left[\frac{\omega \sqrt{\gamma}}{\lambda f K_F (1 - \gamma^{-1})} \right]. \quad (5.11)$$

This approximation becomes more precise when $\omega \rightarrow 0$ (as $l \rightarrow 0$ for constant speed U), consistent with Munk *et al.* (1970).

5.6. Further limiting cases of interest

Rotational effects are assumed to be important if the forcing length scale, L , is greater than half of the Rossby radius of deformation in shallow water, L_r (i.e. if $L > c_s/(2f)$). Thus if $\omega/f > 4\pi Fr_s$ the rotation can be safely neglected and the critical angle θ_{crit2} becomes θ_{trapT} (i.e. the Kelvin mode is replaced by the fundamental edge wave mode).

For $\gamma \gg 1$ (i.e. $h_d \gg h_s$), the angle for the DKW mode becomes the same as for the KW mode, $\theta_{dk} \approx \theta_{crit1}$, consistent with Longuet-Higgins (1968a). When $\theta \rightarrow 0$, only the leaky mode can be excited by super-inertial disturbances (figure 7a-c) and no wave modes can be excited at sub-inertial frequencies, except for the unrealistic case of infinite depth h_d (as $\theta_{crit1} \rightarrow 0$). When $\theta \rightarrow 90^\circ$, depending on γ and $K_F W$, all the wave modes described here can be excited, consistent with Mysak (1969) for DKWs, Thomson (1970) for Kelvin waves and, for instance, Munk *et al.* (1970) for edge and shelf waves. For a super-inertial disturbance propagating along the shelf, wave mode excitation can occur only if $Fr_s > 1$ (figure 7c). If $1 < \omega/f < (\tilde{L}_s^{-2} + 1)^{1/2}$, only the Kelvin / fundamental edge wave mode can be excited (because θ_{trapT} is real and smaller than 90° in 4.5). If $\omega/f > (\tilde{L}_s^{-2} + 1)^{1/2}$, an infinite set of edge waves can be excited, consistent with Snodgrass *et al.* (1962) and Munk *et al.* (1970).

6. Discussion

The previous sections show that different kinds of resonance and amplification of transient waves generated by atmospheric disturbances occur for different topographic scenarios depending on multiple variables: disturbance incident angle, frequency and width, as well as Froude number and Rossby radius of deformation. Table 1 summarizes the modes that can be excited on a step shelf for a range of incident angles, considering both sub- and super-inertial disturbances.

LeBlond & Mysak (1978, p. 553) demonstrated theoretically that the longshore component of the wind stress evaluated at the coast is the primary forcing mechanism for low-frequency shelf waves, for any storm incident angle. Adding to this, it is shown here that the shelf wave amplitude can be enhanced due to resonance for a specific large incident angle (figure 7e). This remark is also valid for super-inertial disturbances generating edge-waves but for smaller incident angles (figure 7a-c). Huthnance (1975) demonstrated the existence of three types of barotropic trapped modes on any straight continental shelf of monotonic depth profile: an infinite discrete set of sub-inertial ‘continental-shelf waves’, a single low-frequency, low wavenumber Kelvin wave and an infinite discrete set of super-inertial ‘edge waves’. Here, for a step shelf profile, only the first-mode shelf wave can be excited (Larsen 1969; Munk *et al.* 1970) and only at sub-inertial frequencies. In addition, a unique sub-inertial DKW mode can be excited on a step shelf.

The forced wave analyzed in this paper is assumed to have a sinusoidal form with

[H]

TABLE 1. Wave modes that can be excited by a super- and sub-inertial atmospheric disturbance crossing a step shelf with an incident angle θ .

Frequency	Incident angle	Wave mode excitation
$\omega > f$	$\theta_{trapR} < \theta < \theta_{trapT}$ $ \theta < \theta_{trapR}$ $\theta_{crit1} < \theta < \theta_{crit2}$ $\theta_{crit1} < \theta < 90^\circ$	Edge wave modes (figure 7a-c) Leaky mode (figure 7a-c) KW mode (figure 7a,b) KW mode, only if $Fr_s > 1$ (figure 7c)
$\omega < f$	$\theta_{crit1} < \theta \leq \theta_{dk}$ $\theta_{crit1} \leq \theta < \theta_{crit2}$ $\theta_{crit1} \leq \theta < 90^\circ$	DKW mode, only if $Fr_s > Fr_{s(min)}$ (figure 7e,f) KW mode, only if $Fr_s < Fr_{s(min)}$ (figure 7d) Shelf mode, only if $Fr_{s(min)} < Fr_s < 1$ and $\omega < f(\gamma - 1)/(\gamma + 1)$ (figure 7e)

wavefronts parallel to each other (equation (2.8)), which could be induced by certain types of atmospheric disturbance (i.e. atmospheric gravity waves, atmospheric jumps) considering minor wind stress effects. Nevertheless, the forced wave induced by an atmospheric cyclonic motion (i.e. hurricane) is more closely represented by a two-dimensional Gaussian-type shape with finite diameter. Although the direction spectra of the forced wave have a higher amplification in the direction of its propagation, it radiates/spreads in a range of directions (similar to the swell energy). Thus, a moving storm crossing the coast or shelf break is able to generate resonance even if its incident angle does not match precisely the resonant conditions found in this study. However, the transient amplification will be stronger for a disturbance with incident angle at or near the critical angle. Figure 7 shows that as the disturbance time scale increases (i.e. as $K_F W$ decreases), the range of angles over which the sea level is significantly amplified expands.

Storms generate ocean waves at all frequencies. However, the predominant response depends strongly on the duration of the passage of the atmospheric forcing over a fixed location (Gordon & Huthnance 1987; Tang *et al.* 1998; Ke & Yankovsky 2011). Thus it is important to distinguish a storm as a super- or sub-inertial disturbance, depending on its passage time.

6.1. Super-inertial responses

Edge waves can be generated only by super-inertial disturbances (i.e. small fast moving storms). They can propagate with the coast either on their right or left. Yankovsky (2009)'s numerical experiments supported an interpretation of the alongshore storm surge evolution induced by Hurricane Wilma's landfall on the west coast of Florida in 2005 as the generation of a large spatial and temporal scale edge wave of period ≈ 6 h and propagation speed $O(10 \text{ m s}^{-1})$. Yankovsky (2009) showed that a fast-moving storm system crossing a sloping shelf profile at a right angle produces a nearly symmetrical response of two edge wave trains propagating in both directions. When the storm's incident angle deviates from the normal approach, most of the edge wave energy propagates in the direction of the alongshore component of the forced wave's translation velocity. Here we add that, using a step shelf profile, the leaky mode will be preferentially excited by a normally incident forced wave. Therefore, storms crossing the shelf with inclined angles

can plausibly cause greater surges and are more likely to retain higher edge wave energy within the shelf after the storm passage.

Fritz *et al.* (2007) and Irish *et al.* (2008) made a storm surge comparison between Hurricane Katrina, reaching Category 5 intensity (Saffir-Simpson Hurricane Scale) over the central Gulf of Mexico and weakening to a Category 3 at landfall (2005), and Camille (Category 5 at landfall, 1969). Both hurricanes moved at similar speeds over the shelf, approximately 6.7 m s^{-1} , but had slightly different tracks and incident angles (Fritz *et al.* 2007, figure 1). Fritz *et al.* (2007) attributed the massive storm surge produced by Katrina to the huge size of the storm and the large northward-propagating swells generated in the hours before landfall. The numerical simulations of Irish *et al.* (2008) demonstrated that storm size plays an important role in hurricane surge generation in coastal areas. Here it is suggested that the different angles of incidence combined with the widths of the hurricanes have played an important role in the enhancement of Katrina's storm surge. Using RMW and central atmospheric pressure values of Irish *et al.* (2008) and applying (2.20) with $C = 1.79$, Katrina ($L \approx 175 \text{ km}$) and Camille ($L \approx 79 \text{ km}$) both had super-inertial frequencies, $\omega/f \approx 3$ and 7 , respectively. It is possible that Camille excited principally the leaky mode when it crossed the shelf break almost at right angles. Energy may have spread in all directions away from the coast. However, considering an ideal step shelf of the area ($h_s = 25 \text{ m}$, $h_d = 2500 \text{ m}$ and $W = 140 \text{ km}$), the second edge wave mode would have been predominantly excited by the passage of Camille. Hurricane Katrina crossed the shelf break with a slightly inclined angle ($\theta \approx 15^\circ$) and the fundamental edge-wave mode was more likely to be excited.

The recent fast moving storm Xynthia which hit the west coast of France had an unexpected large surge on the west coast of France (Grumm 2010). The storm's forward speed was approximately 20 m s^{-1} and its minimal surface atmospheric pressure was about 967 hPa at landfall. Using (2.19) and (2.20) with $C = 1.85$, Xynthia's length scale was roughly 300 km, which gives $\omega/f \approx 4$. The storm crossed the shelf break nearly at right angles. In order to crudely represent the topography under the storm track off the west coast of France, a step shelf ($h_s = 100 \text{ m}$, $h_d = 5000 \text{ m}$ and $W = 160 \text{ km}$) is considered. The storm's passage over this ideal shelf would result in the excitation of the leaky and/or fundamental edge-wave mode (depending on the energy spread around the principal incident angle), suggesting the enhancement of the expected surge level. The most affected regions were 'Vendee' and 'Charente Maritime'. Stronger wind speeds on the right-hand side of the storm track due to the additional storm forward speed might also be a reason for the exceptional surge recorded in these areas.

6.2. Sub-inertial responses

The most observed barotropic sub-inertial responses of the ocean to large and/or slow moving storms over shelves are in the form of Continental shelf waves (CSWs).

Storm-driven CSWs of frequency of about $0.6f$ were observed and modelled over the Scottish continental shelf (Gordon & Huthnance 1987). The step shelf of the region can be approximated as: $h_s = 150 \text{ m}$, $h_d = 1500 \text{ m}$ and $W = 180 \text{ km}$. Most common storms in this region have a positive incident angle relative to the normal of the shelf break and may lead to resonance with free CSWs. Using the present model, the storm's forward speed, U , and frequency, ω/f , must be smaller than 38.3 m s^{-1} and 0.82 , respectively (table 1). Thus large sub-inertial frequency storms are likely to respect those limiting values and excite the shelf wave mode.

Thiebaut & Vennell (2010) noted a fast sub-inertial barotropic continental shelf wave that propagated along the Atlantic coast of Canada after Hurricane Florence crossed the Newfoundland shelf with a forward speed of $\approx 11 \text{ m s}^{-1}$ and time scale of 26–30h (i.e.

$\omega/f \approx 0.6$). The response of the sea surface was observed at the coast and interpreted as the generation of a CSW. The incident angle of Hurricane Florence was far from the resonant angle for shelf wave excitation, which suggests that energy from the finite breadth disturbance was spread across many directions.

Storm surges generated by sub-inertial disturbances can plausibly be enhanced by the excitation of the DKW and CSW modes.

Signorini *et al.* (1992) used numerical simulations to study hurricane-induced surges and currents on the Texas-Louisiana shelf. They pointed out that the range of storm angles associated with the maximum surge generation is within 20° counterclockwise from the shore-normal direction, consistent with the critical angle for sub-inertial resonance (DKW mode excitation) found in sections 4 and 5, assuming $Fr_d < 0.342$ and a sufficiently large step.

As-Salek & Yasuda (2001) used a numerical model to study the effects of cyclone landfall on the Noakhali–Cox’s Bazar coast of Bangladesh. They found that the highest surges are induced by slow moving cyclones with a large radius, making landfall in the northernmost estuary with a small crossing angle ($\approx 30^\circ$) with the coastline (i.e. $\theta \approx 60^\circ$ here). Using an ideal step shelf of the region ($h_s = 120$ m, $h_d = 1500$ m and $W = 150$ km) the present model demonstrates that a sub-inertial disturbance ($\omega/f = 0.8$) of large length scale ($L = 500$ km) crossing the shelf break can excite the shelf wave mode and the maximum response occurs when the incident angle θ approaches 60° .

6.3. Further remarks

In the present formulation, due to the choice of simple step shelf topography, a single shelf wave mode exists (e.g. Larsen 1969; Munk *et al.* 1970). However an infinite number of shelf wave modes can be excited for the case of a more realistic sloping shelf (e.g. Huthnance 1975; Carton 1984) or exponential shelf profile (e.g. Buchwald & Adams 1968; Munk *et al.* 1970).

Furthermore, the vertical cliff considered in this paper (figure 3) is a crude approximation of a shelf break in a real ocean and results show the response of a unique trapped double Kelvin wave. Longuet-Higgins (1968b) showed the existence of an infinite set of trapped progressive waves along a more realistic seascarp where the depth varies continuously, in a zone separating two regions of different depths. He found that in the limit as the transition region tends to zero, the lowest-mode wave reduces to a double Kelvin wave while the higher-mode waves become steady currents. More work is required to investigate the possible infinite set of DKW responses to atmospheric disturbances crossing a smooth continuous depth profile.

As discussed by V07 and V10, the enhancement of Proudman resonance (here MPR) develops slowly after a storm crosses the shelf break. The amplitudes of the forced and transmitted waves are of opposite signs at the shelf break. Thus the MPR effect on the resulting sea level is reduced by the (depressed) transmitted wave. The forced and transmitted waves separate on the shelf due to their differing speeds and propagation directions. V07 showed that near-critical storms require a very wide shelf to fully develop the enhanced forced wave. The separation develops more quickly for very slow or very fast disturbances, allowing narrow shelves to enhance the Proudman resonance. However, this enhancement is small for non-critical storms (V07;V10). V10 pointed out that the separation occurs more rapidly for storms crossing the shelf break near the critical angle and can provoke a larger surge at the coast, even for narrow shelves. The same feature is detected here for super-inertial disturbances with incident angle near θ_{trapT} (figure 8a). Nevertheless, it does not correspond to the critical incident angle θ_{crit} for which MSCR occurs (which was the same as θ_{trapT} in V10). Therefore, even if the separation

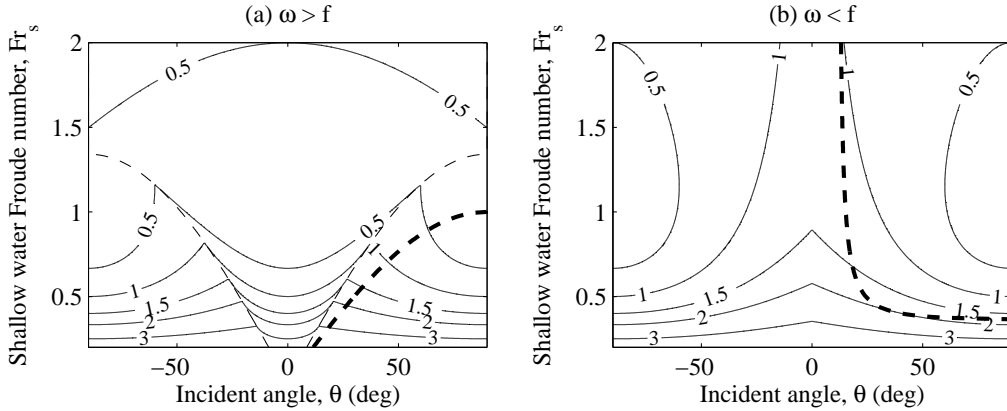


FIGURE 8. Distance (relative to L) between the center of a (a) super- ($\omega/f = 1.5$) and (b) sub-inertial ($\omega/f = 0.5$) frequency storm crossing the shelf and the corresponding transmitted wave after a time equivalent to one time scale T_p . Thick dashed lines represent the critical angles for (a) MSCR, θ_{crit} , and (b) sub-inertial DKW resonances, θ_{dk} . Thin dashed lines in (a) are the trapped angles.

is faster near θ_{trapT} , the resulting surge is expected to be relatively small compared to a disturbance with incident angle near θ_{crit} over a shelf of larger width. For sub-inertial disturbances (figure 8b), the fastest separation occurs when the storm crosses the shelf at right angles. But again the DKW resonance cannot occur for this incident angle. Thus for the same Fr_s , a storm crossing the shelf near the resonant angle θ_{dk} needs more time to fully develop the transient wave compared to normal incidence, but the resulting surge may be larger once developed.

Rego & Li (2009) used a storm surge numerical model and found that increasing the translation speed of the storm decreases flooded volumes while increasing peak surges. This could be explained by the fact that a faster storm is more likely to generate the modified Proudman resonance creating a strong sea level increase but with a high frequency motion (involving smaller water volume for each oscillation). A slower storm is able to generate low-frequency wave-modes, involving a larger volume of water.

In this study, on-shore moving disturbances are considered because they are usually the most devastating events, mostly due to the additional wind induced by the storm translation speed (which is not taken into account here). However, the analytical resonant conditions found for three scenarios apply also for offshore-moving disturbances, with opposite propagation direction affecting only the sign or phase of the transients (V10).

7. Conclusion

In a rotating ocean, the forced wave induced by a moving atmospheric disturbance can lead to several resonances as it crosses a coast, a step or a shelf. When including the effects of the Earth's rotation, the traditional Proudman resonance is replaced by the Modified Proudman Resonance (MPR), which occurs only for a Froude number greater than unity due to the effects of the dimensionless disturbance width (\tilde{L}). The MPR is independent of the disturbance incident angle and can occur only for super-inertial disturbances.

When a storm crosses a vertical coast, sub-critical resonance can occur for a critical positive incident angle $\theta_{crit} = \sin^{-1} Fr$ for which the transient is trapped along the

coast. This is interpreted as a modified version of sub-critical resonance suggested by V10, MSCR, which occurs when the alongshore phase speed of the forced wave matches the free Kelvin-wave phase speed.

Here a new resonance at sub-inertial frequencies is shown to occur as a storm passes over a sufficiently large step with a critical incident angle θ_{dk} (4.14). The existence of this sub-inertial resonance is consistent with the excitation of double Kelvin waves found by Longuet-Higgins (1968a).

For a step shelf, the three resonances still occur at the shelf break and the coast. Nevertheless, the incident angle for strong transient energy can be affected by the finite width of the shelf, resulting in the possible additional excitation of a unique sub-inertial continental shelf wave. Sub- and super-inertial storms crossing a shelf have distinct critical incident angles, dependent on several parameters (Froude numbers on both sides of the step, storm speed, storm time scale, shelf width, local inertial frequency), which can generate large transients travelling along the shelf, enhancing the resulting storm surge at the coast.

For the rotationally influenced forced wave with parallel wavefronts, the Kelvin, double Kelvin and shelf wave can only be excited by disturbances with positive (negative) alongshore wavenumber in the Northern (Southern) Hemisphere. For a more realistic two-dimensional circular Gaussian disturbance, transients are also generated by disturbances with incident angle deviating from the critical angles but may have smaller amplitude. Transients generated by a super-inertial disturbance can travel in both directions along the shelf/coast and can be further magnified by the MPR for Froude numbers approaching $(1 - f^2/\omega^2)^{-1/2}$. Sub-inertial disturbances can only generate transients propagating with the coastline on their right (left) in the Northern (Southern) Hemisphere and no MPR is possible.

Comments from Daryl Coup and the reviewers were much appreciated.

REFERENCES

- ADAMS, J. K. & BUCHWALD, V. T. 1969 The generation of continental shelf waves. *J. Fluid Mech.* **35**, 815–826.
- AS-SALEK, J. A. & YASUDA, T. 2001 Tide-surge interaction in the Meghna estuary: Most severe conditions. *J. Phys. Oceanogr.* **31** (10), 3059–3072.
- BUCHWALD, V. T. & ADAMS, J. K. 1968 The propagation of continental shelf waves. *Proc. Roy. Soc. Lond. A* **305**, 235–250.
- CARTON, J. A. 1984 Coastal circulation caused by an isolated storm. *J. Phys. Oceanogr.* **14** (1), 114–124.
- CHARNOCK, H. 1955 Wind stress on a water surface. *Quart. J. Roy. Meteor. Soc.* **81** (350), 639–640.
- DEFANT, A. 1961 *Physical oceanography*. Pergamon Press.
- DOODSON, A. T. 1924 Meteorological Perturbations of Sea-Level and Tides. *Geophys. J. Int.* **1** (s4), 124–147.
- EKMAN, V. W. 1905 On the influence of the Earth's rotation on ocean currents. *Ark. Mat. Astron. Fys.* **2** (11), 1–53.
- FRITZ, H. M., BLOUNT, C., SOKOLOSKI, R., SINGLETON, J., FUGGLE, A., MCADOO, B. G., MOORE, A., GRASS, C. & TATE, B. 2007 Hurricane Katrina storm surge distribution and field observations on the Mississippi barrier islands. *Estuar. Coast. Shelf Sci.* **74** (1-2), 12–20.
- GARRATT, J. R. 1994 *The atmospheric boundary layer*. Cambridge Univ. Pr.
- GARRETT, C. J. R. 1970 A theory of the Krakatoa tide gauge disturbances. *Tellus* **22** (1), 43–52.

- GILL, A. E. 1982 *Atmosphere-ocean dynamics*. Academic Pr.
- GILL, A. E. & SCHUMANN, E. H. 1974 The generation of long shelf waves by the wind. *J. Phys. Oceanogr.* **4**, 83–90.
- GORDON, R. L. & HUTHNANCE, J. M. 1987 Storm-driven continental shelf waves over the Scottish continental shelf. *Cont. Shelf Res.* **79**, 1015–1048.
- GORING, D. G. 2009 Meteotsunami resulting from the propagation of synoptic-scale weather systems. *Phys. Chem. Earth* **34** (17–18), 1009–1015.
- GREENSPAN, H. P. 1956 The generation of edge waves by moving pressure distributions. *J. Fluid Mech.* **1** (06), 574–592.
- GRUMM, R. H. 2010 The Devastating Western European Winter Storm 27–28 February 2010. National weather service, noaa, web-base interface available at [<http://nws.met.psu.edu/severe/2010/28feb2010.pdf>].
- HOLLAND, G. J. 1980 An analytic model of the wind and pressure profiles in hurricanes. *Mon. Wea. Rev.* **108** (8), 1212–1218.
- HUTHNANCE, J. M. 1975 On trapped waves over a continental shelf. *J. Fluid Mech.* **69** (04), 689–704.
- IRISH, J. L., RESIO, D. T. & RATCLIFF, J. J. 2008 The influence of storm size on hurricane surge. *J. Phys. Oceanogr.* **38**, 2003–2013.
- JAROSZ, E., MITCHELL, D. A., WANG, D. W. & TEAGUE, W. J. 2007 Bottom-up determination of air-sea momentum exchange under a major tropical cyclone. *Science* **315** (5819), 1707.
- JOHNS, B. & LIGHTHILL, J. 1993 Modelling of storm surges in the bay of bengal. In *Tropical Cyclone Disasters*. J. Lighthill et al., Eds., Peking University Press, 410–422.
- KAJIURA, K. 1962 A note on the generation of boundary waves of Kelvin type. *J. Oceanog. Soc. Japan* **18**, 49–58.
- KE, Z. & YANKOVSKY, A. 2011 Relative role of subinertial and superinertial modes in the coastal long wave response forced by the landfall of a tropical cyclone. *Cont. Shelf Res.* **in press**.
- LAMB, H. 1932 *Hydrodynamics*, 6th edn. Cambridge Univ. Pr.
- LARGE, W. G. & POND, S. 1981 Open ocean momentum flux measurements in moderate to strong winds. *J. Phys. Oceanogr.* **11** (3), 324–336.
- LARSEN, JC 1969 Long waves along a single-step topography in a semi-infinite uniformly rotating ocean. *J. Mar. Res.* **27** (1), 1–6.
- LEBLOND, P. H. & MYSAK, L. A. 1978 *Waves in the Ocean*. Elsevier Oceanography Series.
- LIGHTHILL, J. 1998 Fluid mechanics of tropical cyclones. *Theor. Comp. Fluid Dyn.* **10** (1), 3–21.
- LONGUET-HIGGINS, M. S. 1968a On the trapping of waves along a discontinuity of depth in a rotating ocean. *J. Fluid Mech.* **31** (03), 417–434.
- LONGUET-HIGGINS, M. S. 1968b Double Kelvin waves with continuous depth profiles. *J. Fluid Mech.* **34** (01), 49–80.
- MAKIN, V. K. 2005 A note on the drag of the sea surface at hurricane winds. *Bound.-Layer Meteor.* **115** (1), 169–176.
- MERCER, D., SHENG, J., GREATBATCH, R. J. & BOBANOVIC, J. 2002 Barotropic waves generated by storms moving rapidly over shallow water. *J. Geophys. Res.* **107**, 31523168.
- MONSERRAT, S., IBBETSON, A. & THORPE, A. J. 1991 Atmospheric gravity waves and the rissaga phenomenon. *Q. J. Roy. Meteorol. Soc.* **117**, 553–570.
- MONSERRAT, S., VILIBIĆ, I. & RABINOVICH, A. B. 2006 Meteotsunamis: atmospherically induced destructive ocean waves in the tsunami frequency band. *Nat. Hazards Earth Syst. Sci.* **6**, 1035–1051.
- MOON, I. J., GINIS, I. & HARA, T. 2004 Effect of surface waves on air–sea momentum exchange. Part II: Behavior of drag coefficient under tropical cyclones. *J. Atmos. Sci.* **61**, 2334–2348.
- MUNK, W., SNODGRASS, F. & WIMBUSH, M. 1970 Tides off-shore: Transition from California coastal to deep-sea waters. *Geophys. Fluid Dyn.* **1** (1), 161–235.
- MYSAK, L. A. 1967a On the theory of continental shelf waves. *J. Mar. Res.* **25**, 205–227.
- MYSAK, L. A. 1967b On the very low frequency spectrum of the sea level on a continental shelf. *J. Geophys. Res.* **72**, 3043–3047.
- MYSAK, L. A. 1969 On the generation of double Kelvin waves. *J. Fluid Mech.* **37** (03), 417–434.
- MYSAK, L. A. 1980 Recent advances in shelf wave dynamics. *Rev. Geophys.* **18** (1), 211–241.

- NOMITSU, T. 1935 A theory of tsunamis and seiches produced by wind and barometric gradient. *Mem. Coll. Sci. Imp. Univ. Kyoto A* **18**, 201–214.
- POWELL, M. D. 1980 Evaluations of diagnostic marine boundary-layer models applied to hurricanes. *Mon. Weather Rev.* **108**, 757–766.
- POWELL, M. D., VICKERY, P. J. & REINHOLD, T. A. 2003 Reduced drag coefficient for high wind speeds in tropical cyclones. *Nature* **422** (6929), 279–283.
- PROUDMAN, J. 1953 *Dynamical Oceanography*. Wiley and Sons.
- RABINOVICH, A. B. & MONSERRAT, S. 1996 Meteorological tsunamis near the Balearic and Kuril Islands: Descriptive and statistical analysis. *Natural Hazards* **13** (1), 55–90.
- REGO, J. L. & LI, C. 2009 On the importance of the forward speed of hurricanes in storm surge forecasting: A numerical study. *Geophys. Res. Lett.* **36** (7), L07609.
- ROBINSON, A. R. 1964 Continental shelf waves and the response of sea level to weather systems. *J. Geophys. Res.* **69**, 367–368.
- SIGNORINI, S. R., WEI, J. S. & MILLER, C. D. 1992 Hurricane-induced surge and currents on the Texas-Louisiana shelf. *J. Geophys. Res.* **97** (C2), 2229–2242.
- SIMPSON, R. H. 1974 The hurricane disaster potential scale. *Weatherwise* **27** (8), 169 and 186.
- SMITH, S. D. & BANKE, E. G. 1975 Variation of the sea surface drag coefficient with wind speed. *Quart. J. Roy. Meteor. Soc.* **101** (429), 665–673.
- SNODGRASS, F. E., MUNK, W. H. & MILLER, G. R. 1962 Long-period waves over Californias continental borderland. Part I. Background spectra. *J. Mar. Res.* **20**, 3–30.
- TANG, C. L., GUI, Q. & DETRACEY, B. M. 1998 Barotropic Response of the Labrador/Newfoundland Shelf to a Moving Storm. *J. Phys. Oceanogr.* **28**, 1152–1172.
- TEAGUE, W. J., JAROSZ, E., WANG, D. W. & MITCHELL, D. A. 2007 Observed Oceanic Response over the Upper Continental Slope and Outer Shelf during Hurricane Ivan*. *J. Phys. Oceanogr.* **37**, 2181–2206.
- THIEBAUT, S. & VENNEL, R. 2010 Observation of a fast continental shelf wave generated by a storm impacting Newfoundland using wavelet and cross wavelet analyses. *J. Phys. Oceanogr.* **40** (2), 417–428.
- THOMSON, R. E. 1970 On the generation of Kelvin-type waves by atmospheric disturbances. *J. Fluid Mech.* **42** (4), 657–670.
- VALLIS, G.K. 2006 *Atmospheric and oceanic fluid dynamics: fundamentals and large-scale circulation*. Cambridge Univ. Press.
- VENNEL, R. 2007 Long Barotropic Waves Generated by a Storm Crossing Topography. *J. Phys. Oceanogr.* **37**, 2809–2823.
- VENNEL, R. 2010 Resonance and trapping of topographic transient ocean waves generated by a moving atmospheric disturbance. *J. Fluid Mech.* **650**, 427–442.
- VICKERY, P. J. & WADHERA, D. 2009 Statistical Models of Holland Pressure Profile Parameter and Radius to Maximum Winds of Hurricanes from Flight-Level Pressure and H* Wind Data. *J. Appl. Meteorol. Climatol.* **47** (10), 2497–2517.
- VILIBIĆ, I., MONSERRAT, S., RABINOVICH, A. & MIHANOVIĆ, H. 2008 Numerical Modelling of the Destructive Meteotsunami of 15 June, 2006 on the Coast of the Balearic Islands. *Pure Appl. Geophys.* **165** (11), 2169–2195.
- WEISBERG, R. H. & ZHENG, L. 2006 Hurricane storm surge simulations for Tampa Bay. *Estuar. Coasts* **29** (6), 899–913.
- WU, J. 1982 Wind-stress coefficients over sea surface from breeze to hurricane. *J. Geophys. Res.* **87** (C12), 9704–9706.
- XIE, L., PIETRAFESA, L. J. & ZHANG, C. 1999 Subinertial response of the Gulf Stream system to Hurricane Fran of 1996. *Geophys. Res. Lett.* **26** (23), 3457–3460.
- YANKOVSKY, A. E. 2008 Long-Wave Response of the West Florida Shelf to the Landfall of Hurricane Wilma, October 2005. *J. Coast. Res.* **24** (sp3), 33–39.
- YANKOVSKY, A. E. 2009 Large-scale edge waves generated by hurricane landfall. *J. Geophys. Res., C* **114** (C3), C03014.